

# The Impact of Lightning Data Assimilation on Deterministic and Ensemble Forecasts of Convective Events

KEN DIXON, CLIFFORD F. MASS, GREGORY J. HAKIM, AND ROBERT H. HOLZWORTH

*University of Washington, Seattle, Washington*

(Manuscript received 18 September 2015, in final form 29 April 2016)

## ABSTRACT

A general lightning data assimilation technique is developed and tested with observations from the World Wide Lightning Location Network (WWLLN). The technique nudges the water vapor mixing ratio toward saturation within 10 km of a lightning observation and is more general than other approaches that require specific model microphysics or flash rates. This approach is applied to both deterministic and ensemble forecasts of the 29 June 2012 derecho event over the eastern United States and a deterministic forecast of the 17 November 2013 convective event over the Midwest using the Weather Research and Forecasting (WRF) Model run at a convection-permitting resolution. Lightning data are assimilated over the first three hours of the forecasts, and the subsequent impact on forecast quality is evaluated. For both events, the deterministic simulations with lightning-based nudging produce more realistic predicted composite reflectivity fields. For the forecasts of the 29 June 2012 event using ensemble data assimilation, forecast improvements from lightning assimilation were more modest than for the deterministic forecasts, suggesting that lightning assimilation may produce greater improvements in convective forecasts where conventional observations (e.g., aircraft, surface, radiosonde, satellite) are less dense or unavailable.

## 1. Introduction

Advances in computing power have made it possible for operational regional forecast systems to reach convection-permitting horizontal grid spacing ( $\Delta x \leq 4$  km), alleviating the need for a cumulus parameterization scheme (CPS) and creating the opportunity to assimilate convective-scale observations to improve forecasts (Weisman et al. 1997; Kain et al. 2008). Today, radar reflectivity and lightning-flash-rate observations are assimilated through latent heating into the operational Rapid Refresh (RAP) and High-Resolution Rapid Refresh (HRRR) forecast systems (Weygandt et al. 2008). As advances in computing power continue, operational global forecast systems are expected to reach convection-permitting horizontal resolutions in the near future, creating a demand for convective-scale observations, particularly over data-sparse regions such as the open ocean.

In recent years, long-range, land-based detection networks, such as the World Wide Lightning Location

Network (WWLLN) operated by the University of Washington and the Global Lightning Dataset (GLD360) operated by Vaisala, have made global lightning detection possible. Furthermore, continuous coverage of lightning activity over much of the Western Hemisphere will soon be available from the Geostationary Lightning Mapper (GLM) aboard the R-Series Geostationary Operational Environmental Satellite (GOES-R), which is expected to launch in 2016 (Goodman et al. 2013). Given the difficulty of acquiring continuous mesoscale observations (e.g., radar or surface) with global coverage and the lack of GOES-R GLM coverage in the Eastern Hemisphere, lightning location information from long-range, land-based lightning networks such as WWLLN could help fill the gap in convective-scale observations available for assimilation on a global scale. Thus, a goal of this research is to evaluate a generally applicable lightning assimilation approach using WWLLN, verifying our results in a region with dense observational assets (the eastern United States).

There have been several attempts to assimilate lightning data into numerical weather prediction systems. A central task of these efforts is to establish a relationship between lightning activity and resolved atmospheric

---

*Corresponding author address:* Clifford F. Mass, Department of Atmospheric Sciences, University of Washington, Box 351640, Seattle, WA 98195-1640.  
E-mail: cmass@uw.edu

variables. Some assimilation experiments have derived regional relationships between flash rate and rainfall rate, and then scaled the vertical latent heating profile based on the inferred rainfall rates (Alexander et al. 1999; Chang et al. 2001; Pessi and Businger 2009). Pessi and Businger (2009), using a long-range lightning detection network, found that forecasts of large-scale fields such as sea level pressure were improved by assimilating lightning; however, the low horizontal resolution of the models employed ( $\Delta x \geq 27$  km) prevented explicit resolution of convection. It is also unclear how relationships between flash rate and rainfall rate, which are known to vary spatially (Petersen and Rutledge 1998), can be applied on a global scale.

A second group of studies assimilated lightning into higher-resolution, but not convection-permitting, regional models ( $\Delta x = 10$  km). In Papadopoulos et al. (2005), model humidity profiles were nudged toward humidity profiles derived from observed soundings when lightning occurred. Although the technique produced improved convective precipitation forecasts during the assimilation period and the subsequent 12-h forecasts, it made use of regionally and seasonally specific moisture profiles, making it difficult to apply globally. Mansell et al. (2007) forced lifting to the level of free convection when lightning was observed and added moisture to lifted parcels to satisfy minimum cloud depth and peak updraft criteria; their approach resulted in improved cold pool representation and subsequent convective initiation. Although these studies improved convective forecasts by assimilating lightning, they relied on CPSs to produce convection and they may not be relevant to simulations at convection-permitting horizontal resolutions.

The first attempt to assimilate lightning using a convection-permitting horizontal grid spacing, by Fierro et al. (2012, 2014;  $\Delta x = 1$  km), modified the water vapor mixing ratio in the mixed-phase region ( $-20^\circ \leq T \text{ }^\circ\text{C} \leq 0^\circ\text{C}$ ), where charge separation is most significant according to noninductive charging theory (Saunders 2008, and references therein). This assimilation technique was motivated by the successful initialization of a high-resolution simulation of Hurricane Rita by saturating vertical levels between 3 and 11 km above the surface in a region where lightning was observed (Fierro and Reisner, 2011). The water vapor mixing ratio was nudged based on observed gridded flash rates of total lightning, with the amount of nudging inversely proportional to the amount of graupel present in a model grid cell. This technique improved the simulation of a line of thunderstorms in Oklahoma, and the 0–6-h forecast of a destructive derecho in the upper Midwest and mid-Atlantic United States on 29 June 2012.

In addition to decreases in horizontal grid spacing, advances in computing power have facilitated high-resolution ensemble forecasting and associated data assimilation techniques, such as the ensemble Kalman filter (EnKF; Evensen 1994) approach, which uses error covariance statistics derived from ensemble members to update model state variables away from the observation location. Assimilating lightning using an EnKF is problematic because it is difficult to specify a forward model; furthermore, the discontinuous nature of convection can result in the rejection of a lightning observation when no ensemble members are producing convection in that location. Thus, an approach is needed to assimilate lightning that is compatible with the assimilation of observations by an EnKF system. An attempt at such a hybrid approach was made by Ballabrera-Poy et al. (2009), which reduced analysis error in the Lorenz and Emanuel (1998) model when including large-scale, slowly evolving observations in EnKF updates and assimilating small-scale observations using nudging.

Given the ease of implementation of observation nudging, as well as the success of moisture nudging in a range of previous high-resolution studies, a lightning data assimilation technique based on moisture nudging is described in this work, using global lightning location data available from WWLLN. For the first time, this technique is tested for both high-resolution deterministic and ensemble forecasts, considering the June 2012 derecho and the 17 November 2013 convective event. The performance of the lightning assimilation technique is assessed based on its impact on a short-term forecast ( $\leq 24$  h) of convective features.

## 2. Data and methods

### a. Lightning data

For this study, lightning location data from WWLLN is employed. WWLLN is a network of approximately 70 sensors that detect sferics; very low-frequency (3–30 kHz) radiation packets produced by lightning strikes. The propagation of sferics within the Earth-ionosphere waveguide allows for the detection of lightning at distances of thousands of kilometers, enabling WWLLN to provide global lightning detection coverage (Dowden et al. 2002).

WWLLN is able to detect both intracloud (IC) and cloud-to-ground (CG) lightning strikes. Since detection efficiency increases with the peak current of lightning strikes, WWLLN is more efficient at detecting CG lightning due to the associated higher peak currents (Jacobson et al. 2006). The detection efficiency of WWLLN is approximately 10%–11%, with

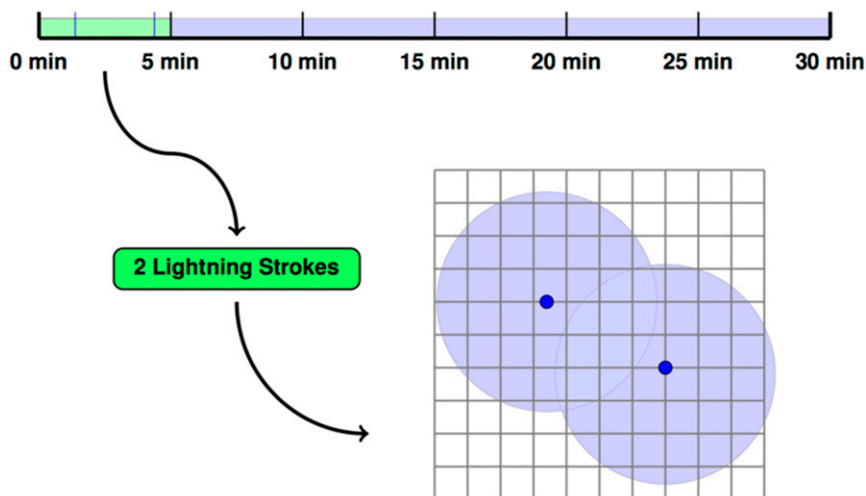


FIG. 1. A schematic of the lightning nudging process. (top) A timeline during a portion of the simulation, divided into 5-min bins. The green highlighting indicates the temporal bin containing the current time step, with blue lines representing observed lightning strikes. (bottom) An example of how the lightning strike locations (blue dots) are used to determine which grid points are nudged on the model domain (points within light blue circles) when the current simulation time step is within the green-highlighted bin.

location errors less than 10 km based on comparisons with observations from the short-range lightning observation networks in North America, which have detection efficiencies exceeding 90% and location accuracies within

1 km (Abarca et al. 2010; Abreu et al. 2010). Despite its modest detection efficiency, WWLLN is highly efficient at detecting lightning-producing storms during 3-h periods (Jacobson et al. 2006).

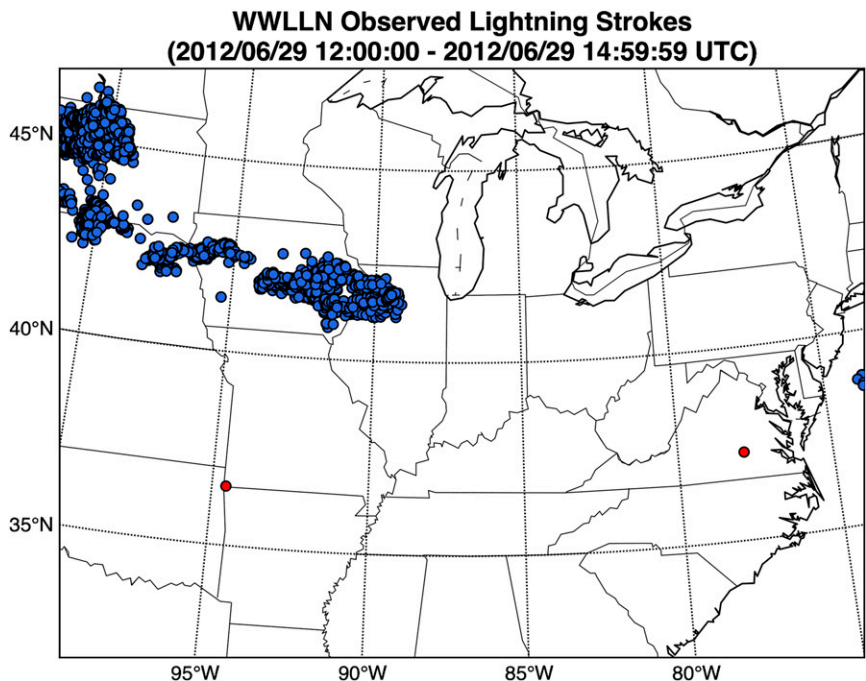


FIG. 2. Lightning strikes observed by WWLLN between 1200 and 1500 UTC 29 Jun 2012 over the WRF domain described in section 2c. Location data from 4315 lightning strikes were assimilated in the NUDGE and ENS-NUDGE experiments (blue dots). Two lightning strikes were removed by the filtering technique described in section 2a (red dots).

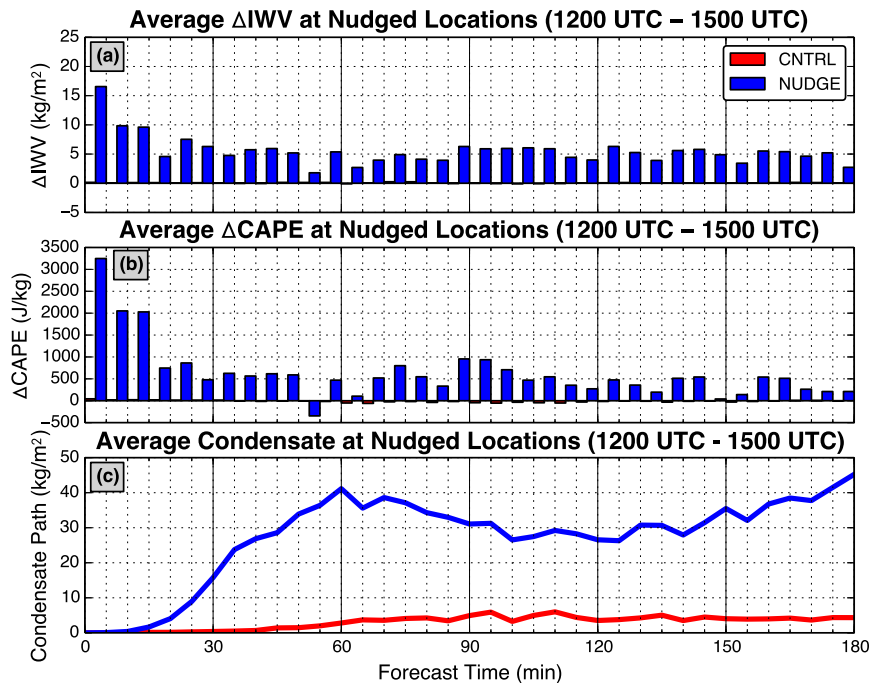


FIG. 3. Average temporal changes in (a) IWV and (b) CAPE at grid points where nudging is performed in NUDGE for the deterministic simulation of the 29 Jun 2012 event. (c) Average column condensate (liquid and solid water path) at nudged locations. Red bars (barely visible) and lines represent results from CNTRL, while blue bars and lines represent results from NUDGE.

Although the time of group arrival technique employed by WWLLN requires four sensors to locate a lightning strike (Dowden et al. 2002), only strikes detected by five or more lightning sensors are retained by WWLLN. To reduce the potential for poorly located lightning strikes, observed lightning events are placed into  $0.5^\circ \times 0.5^\circ$  bins and strikes are removed when no other lightning strike is observed in the same bin, or any adjacent bin, within the previous 60 min. Strikes observed by six or more sensors are exempt from the filtering procedure (R. Holzworth and J. Brundell 2013, personal communication).

#### b. Assimilation technique

Since the Weather Research and Forecasting (WRF) Model does not explicitly forecast lightning, it is necessary to design a way to adjust the simulated atmospheric state toward conditions that are representative of the lightning observed by WWLLN. In this study, a four-dimensional data assimilation technique known as Newtonian relaxation or nudging is applied to lightning data. Specifically, we use the approach of Stauffer and Seaman (1994), which was designed for the assimilation of surface and upper-air measurements of prognostic variables

such as temperature, wind, and water vapor mixing ratio.

As noted above, WWLLN is more efficient at detecting CG lightning than IC lightning, with CG lightning generally occurring after the cloud top has reached its maximum height (Williams et al. 1989; Solomon and Baker 1998). Thus, in this study the water vapor mixing ratio is nudged toward the saturation water vapor mixing ratio (100% relative humidity) at all vertical levels in the troposphere (levels where atmospheric pressure exceeds 200 hPa) within 10 km of any observed lightning strike. Smaller radii and varying nudging tops (50, 500 hPa) were tested, but they did not produce superior performance (more details in section 3b). The addition of moisture decreases the lifting condensation level (LCL) and increases the convective available potential energy (CAPE), encouraging the production of a deep cloud where lightning strikes are observed.

Although some previous studies have used nudging as part of their lightning data assimilation approach (Papadopoulos et al. 2005; Fierro et al. 2012, 2014), the water vapor nudging approach used in this study is substantially different and addresses several limitations of those techniques. First, this approach is independent of parameterized microphysical quantities, unlike the

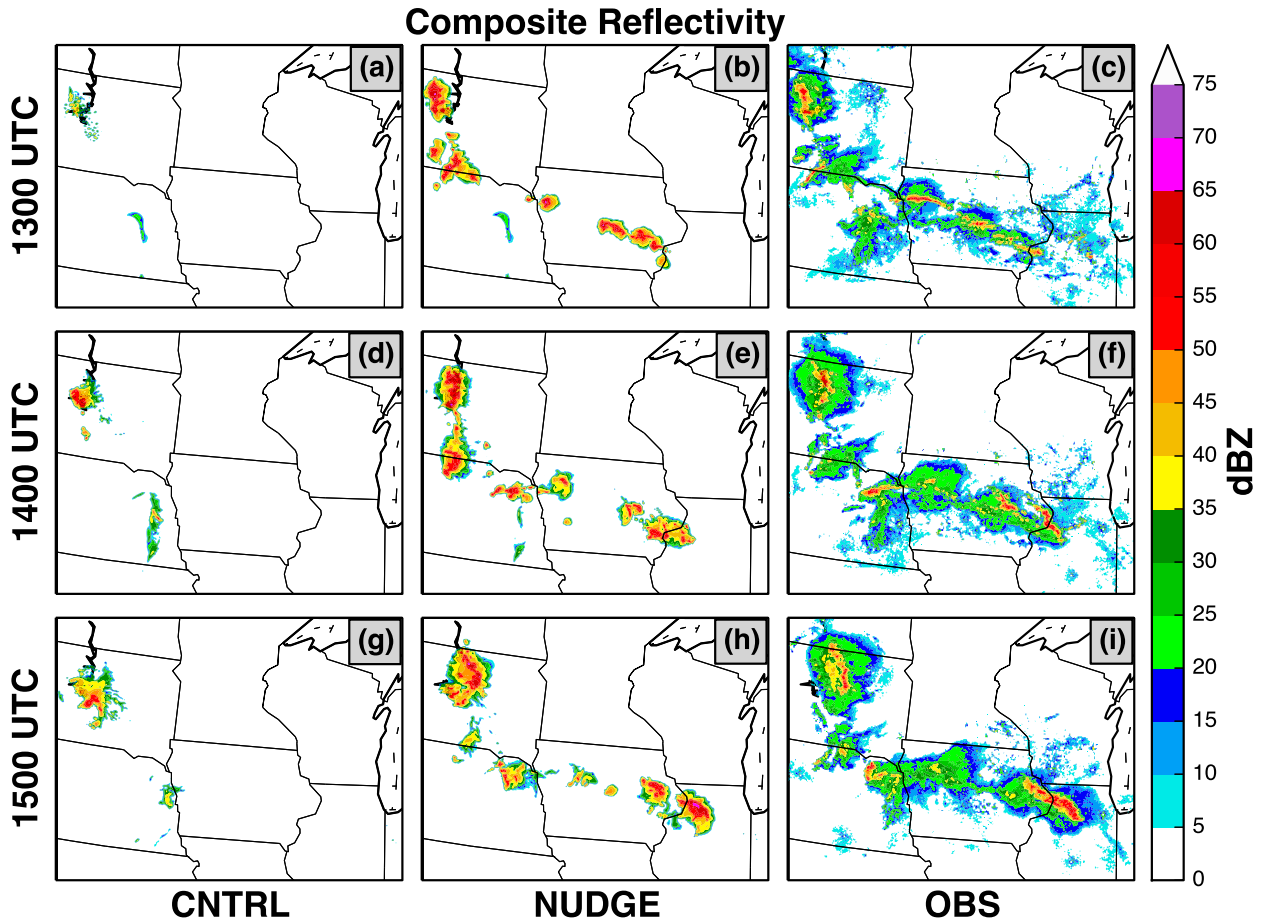


FIG. 4. Simulated and observed composite reflectivity for the first three hours of the deterministic simulations of the 29 Jun 2012 event (1300–1500 UTC 29 Jun 2012) for (a),(d),(g) CNTRL, (b),(e),(h) NUDGE, and (c),(f),(i) observations. The northwest portion of the model domain is displayed.

technique in [Fierro et al. \(2012, 2014\)](#), avoiding the need to establish a relationship between microphysical quantities (e.g., graupel) and lightning. It thus eliminates the need to tune the technique for different microphysics schemes. Second, this approach does not restrict nudging to any vertical layer of the troposphere, instead encouraging both surface-based and elevated convection by nudging the water vapor mixing ratio at all vertical levels within the troposphere. This is in contrast to the assimilation technique of [Fierro et al. \(2012, 2014\)](#), which restricts moisture nudging to the mixed-phase region. Third, this technique nudges moisture, a requirement of convective activity, instead of nudging a quantity such as latent heating, which is a consequence of convective activity ([Alexander et al. 1999](#); [Chang et al. 2001](#); [Pessi and Businger 2009](#)). By taking this approach, there is no need to rely on region-specific relationships between lightning and rainfall or assumed latent heating profiles. Fourth, this technique is independent of the observed flash rate, taking advantage of a simple physical

interpretation of WWLLN-observed lightning strikes that obviates tuning the amount of moisture nudging for spatial variations in flash rates, such as between land-based and ocean-based storms ([Williams et al. 2004](#)). Furthermore, because of the low detection efficiency of WWLLN, particularly over remote regions, flash-rate information will not allow reliable extraction of convective intensity, such as updraft strength. There are, of course, potential drawbacks of this approach. It does not modulate the strength of convection by the lightning flash rate, and small amounts of moisture may be added to the lower stratosphere when the tropopause extends below 200 hPa. The use of a dynamical quantity like potential vorticity may be appropriate for selecting the upper vertical limit for moisture nudging, but as shown below, the impact of changing the vertical limit of nudging is small.

The technique described above is performed using a modified version of the observation nudging described in [Stauffer and Seaman \(1994\)](#) and implemented in WRF by [Liu et al. \(2005\)](#). In our application of observation nudging, WWLLN strikes are binned by 5-min

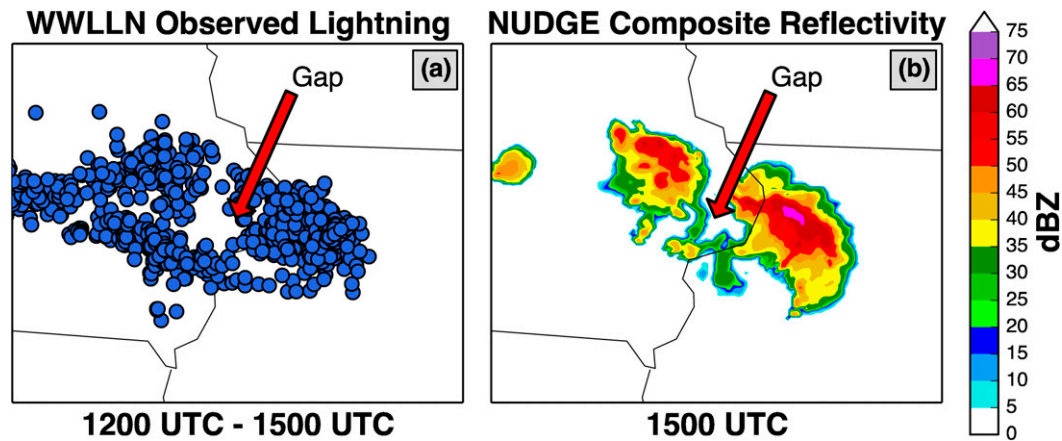


FIG. 5. (a) Lightning strikes observed by WWLLN between 1200 and 1500 UTC over eastern Iowa and western Illinois. (b) Simulated composite reflectivity in NUDGE over the same region at 1500 UTC (at the end of the 3-h nudging period). The red arrow indicates an area location with a lack of WWLLN-observed lightning strikes.

intervals, so grid points are nudged long enough to initiate convection but short enough so that the nudged grid points are representative of the current distribution of thunderstorms and not their path of motion. The quality of the WWLLN lightning strikes (filtered as described in section 2a) is assumed to be perfect, and spatial and temporal weighting functions are modified such that the water vapor mixing ratio at a grid point is nudged only if lightning is observed within 10 km during the current 5-min interval. Nudging occurs only below 200 hPa. A schematic of this weighting approach is presented in Fig. 1. The

relaxation time scale is set to 5 min, which yields a nudging coefficient of  $G = 3.33 \times 10^{-2} \text{ s}^{-1}$ . The nudging term does not depend on the number of lightning strikes within 10 km of a grid point; one is sufficient for maximum effect.

Equation (1) describes the water vapor mixing ratio tendency equation, where  $\mathbf{x}$  is the spatial location of the grid point,  $t$  is time,  $\mathbf{F}(\alpha, \mathbf{x}, t)$  represents the physical forcing terms in the model,  $q_v$  is the model water vapor mixing ratio,  $q_{v,s}$  is the saturation water vapor mixing ratio, and  $d$  is the distance from the grid point to the nearest lightning strike observed in the 5-min bin that includes the current time step,

$$\frac{\partial p^* q_v}{\partial t} = \begin{cases} F(q_v, \mathbf{x}, t) + Gp^*(q_{v,s} - q_v), & (p > 200 \text{ hPa}) \text{ and } (d \leq 10 \text{ km}) \\ F(q_v, \mathbf{x}, t), & \text{otherwise} \end{cases} \quad (1)$$

### c. Model configuration

All numerical weather simulations analyzed in this work are produced using version 3.4 of the Weather Research and Forecasting Model with the Advanced Research dynamics solver (ARW). This is a fully compressible, nonhydrostatic model supported by the Mesoscale and Microscale Meteorology Division (MMM) of the National Center for Atmospheric Research (NCAR; Skamarock et al. 2008).

All simulations are performed on a single domain over the eastern United States with 3-km horizontal grid spacing,  $750 \times 550$  grid points, and 38 vertical levels. The Thompson 6-class bulk microphysics scheme with graupel and double-moment rain and ice is used (Thompson et al. 2008). No convective parameterization scheme is applied, since the horizontal grid spacing is convection permitting. Other parameterizations include the Rapid Radiative

Transfer Model (RRTM) longwave and MM5 shortwave radiation schemes (called every 30 min), as well as the Yonsei University (YSU) boundary layer scheme. The time step is 12 s and boundary conditions are provided every three hours from the National Centers for Environmental Prediction (NCEP) Global Forecast System (GFS) forecast ( $0.5^\circ$  grid) initialized at the same time. To prevent numerical instabilities during data assimilation, vertical motions that result in CFL numbers exceeding one are damped. Additionally, to prevent upper boundary reflection, vertical motions are relaxed toward zero in the upper 7 km of the domain using a coefficient of  $0.2 \text{ s}^{-1}$ .

### 1) DETERMINISTIC EXPERIMENTS

For the deterministic simulations, 24-h forecasts are produced using the WRF configuration described above

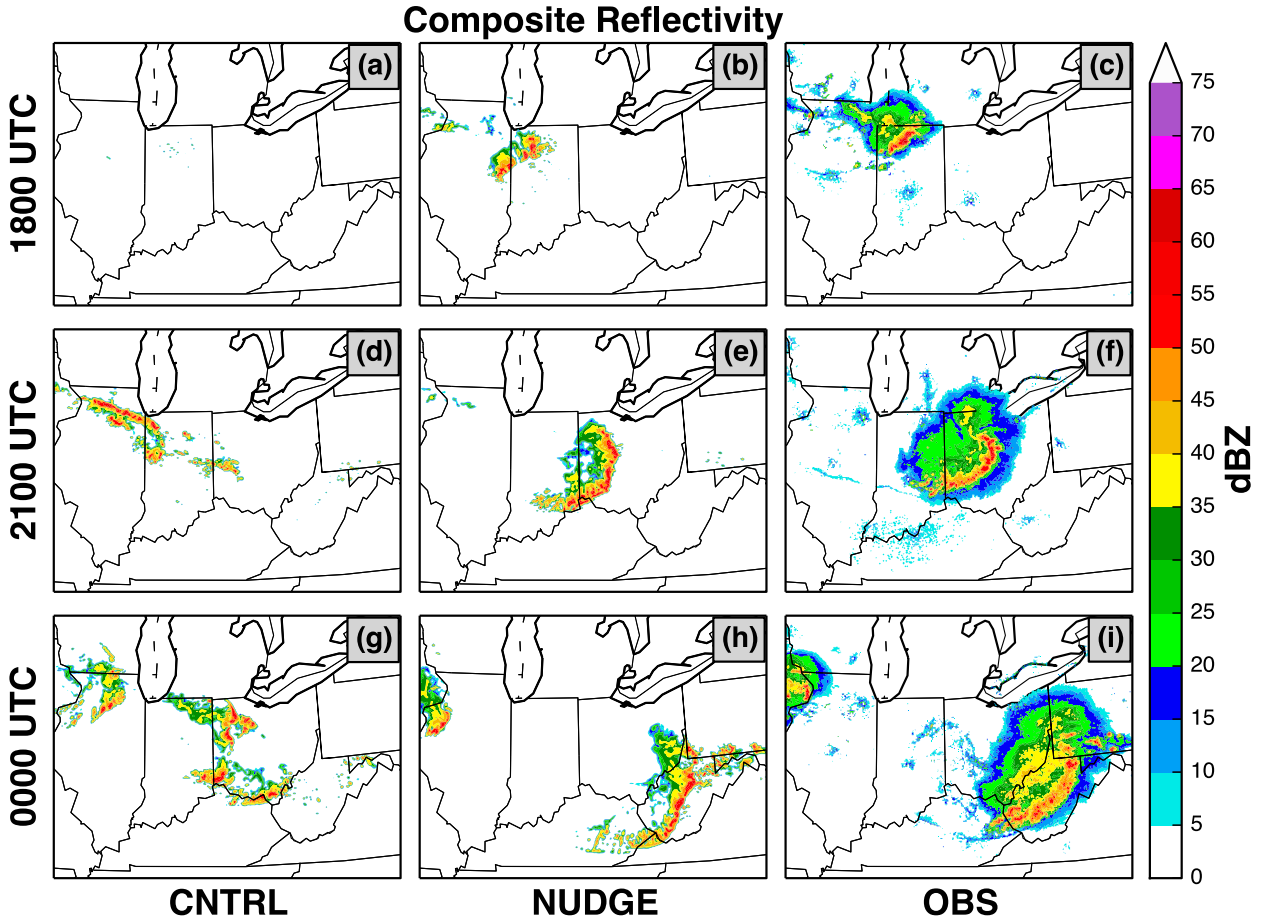


FIG. 6. As in Fig. 4, except results are displayed at 3-h intervals between 1800 UTC 29 Jun and 0000 UTC 30 Jun 2012. The central portion of the model domain is displayed.

with initial conditions from the GFS 0.5° resolution analysis. For all deterministic experiments, two simulations are performed: a control simulation with no data assimilation (labeled as CNTRL) and a simulation with lightning nudging through the first three hours of the simulation, as described in section 2b (labeled as NUDGE).

## 2) ENSEMBLE EXPERIMENTS

An ensemble forecast experiment for the June 2012 derecho is completed using the aforementioned WRF configuration and software provided by the Data Assimilation Research Testbed (DART) group of NCAR. The ensemble adjustment Kalman filter variant of the EnKF (EAKF; Anderson 2001) is used to assimilate observations every three hours, using observations available within 30 min of the assimilation time. Observations for the EnKF assimilation step are obtained from the National Oceanic and Atmospheric Administration’s (NOAA) Meteorological Assimilation Data

Ingest System (MADIS) and include METAR surface data, ship and buoy observations, satellite-observed winds, radiosonde observations, and observations from the Aircraft Communication, Addressing, and Reporting System (ACARS). Observations within five grid points of the lateral boundaries are discarded, as are upper-level observations at altitudes above 20 km or at pressure levels less than 100 hPa. Surface observations with elevations differing by more than 200 m from model terrain elevation are not assimilated. For both aircraft and satellite wind observations, observations of the same source that are within 45 km horizontally and 25 hPa vertically are averaged together to create a superobservation. Any observation more than three standard deviations from the ensemble mean is discarded. To avoid filter divergence, spatially varying inflation is applied to the ensemble prior to EnKF assimilation (Anderson 2009). The Gaspari–Cohn function is used to damp covariances at large distances from observations (horizontal and vertical radii of

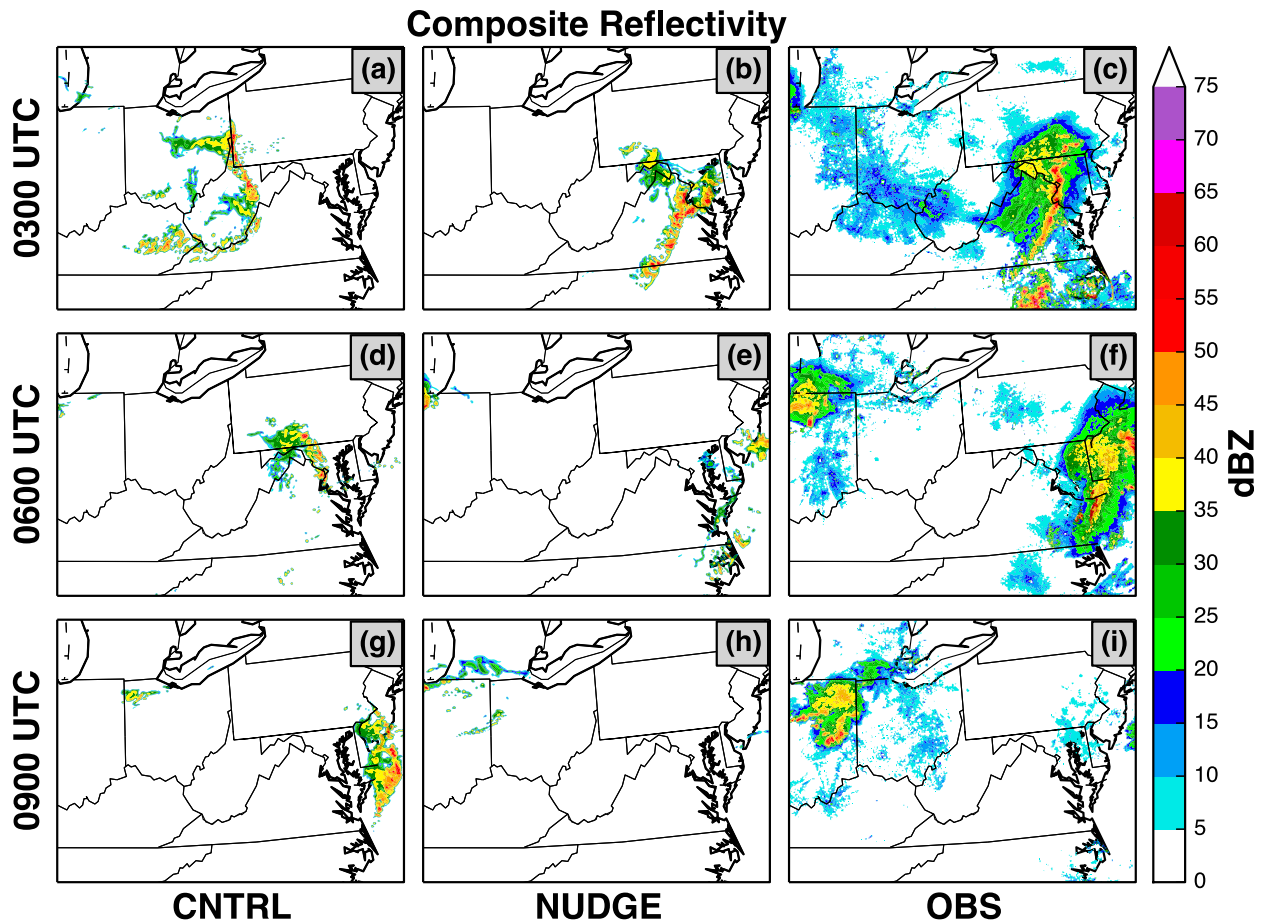


FIG. 7. As in Fig. 4, except results are displayed at 3-h intervals between 0300 and 0900 UTC 30 Jun 2012. The east central portion of the model domain is displayed.

1000 and 16 km, respectively) in order to prevent spurious covariances from affecting the ensemble states at unreasonable distances (Gaspari and Cohn 1999; Hamill et al. 2001). Testing revealed that the results are not sensitive to substantial changes in these damping radii.

For the ensemble experiments, a 64-member ensemble is populated initially by perturbing the GFS  $0.5^\circ$  analysis valid at 1200 UTC 28 June 2012 using version 3.4 of the WRF data assimilation (WRFDA) system maintained by NCAR/MMM. WRFDA perturbs the GFS analysis according to background error covariances estimated from a year of differences in 24- and 48-h GFS forecasts valid at the same time [the covariance option 3 (CV3)]. A 24-h spinup between 1200 UTC 28 June and 1200 UTC 29 June 2012 is performed to develop error covariances that are representative of the uncertainty in the state of the atmosphere at the time of assimilation. To reduce spinup time and lessen the initialization shock, the digital filter initialization option in WRF is applied at 1200 UTC 28 June 2012 using 30 min of

backward integration and 15 min of forward integration (Huang and Yang 2002). For ensemble integrations beginning at 0000, 0600, 1200, and 1800 UTC, boundary conditions are from the GFS forecasts initialized 6 h prior. For ensemble integrations beginning at 0300, 0900, 1500, and 2100 UTC, boundary conditions are from GFS forecasts initialized three hours prior. To maintain ensemble spread, the boundary conditions are perturbed using the fixed covariance perturbation method (Torn et al. 2006). No EnKF assimilation step is performed at 1200 UTC 28 June 2012, and inflation is not introduced until just before the 1800 UTC 28 June 2012 EnKF assimilation step. No moisture nudging is performed during the 24-h spinup period.

After the spinup period, which concludes with an EnKF assimilation step at 1200 UTC 29 June 2012, two versions of the ensemble are run: 1) one without lightning-related moisture nudging, with a final EnKF assimilation step at 1500 UTC 29 June 2012 (ENS-CNTRL); and 2) a run with lightning-related moisture

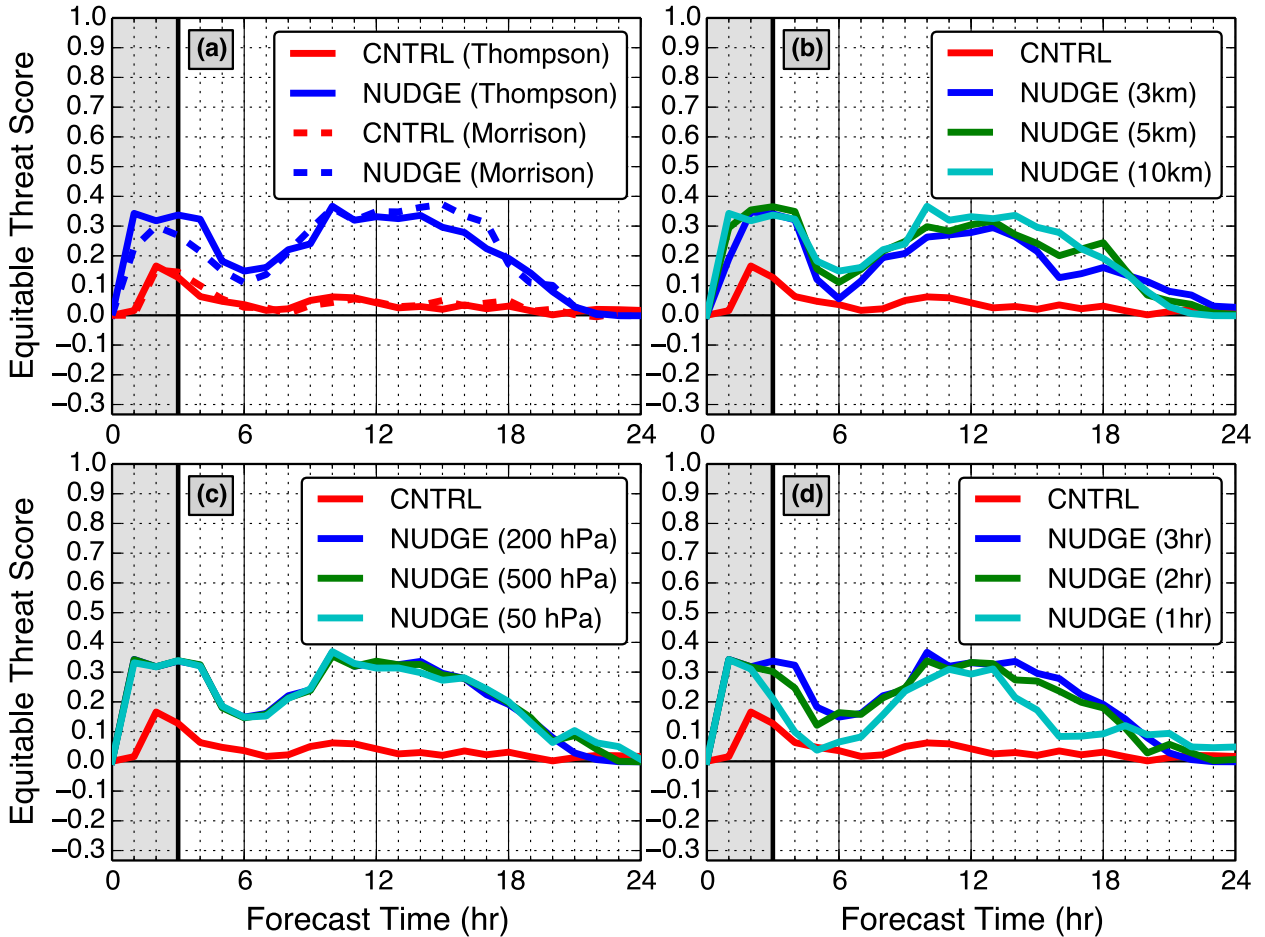


FIG. 8. ETS for precipitation  $\geq 1$  mm for both the control and nudged simulations of the 29 Jun 2012 event, using (a) either Thompson or Morrison microphysics, for various (b) nudging radii, and differing (c) vertical nudging extents and (d) nudging periods. The vertical gray shaded area indicates times of moisture nudging in the NUDGE simulations.

nudging from 1200 to 1500 UTC 29 June 2012, with a final EnKF assimilation step at 1500 UTC 29 June 2012 (ENS-NUDGE).

*d. Evaluation*

To evaluate the numerical forecasts, simulated rainfall is compared to the NOAA stage IV precipitation analysis (Lin and Mitchell 2005). This product combines radar and rain gauge-based precipitation observations and is available on a 4-km grid covering most of the domain described in section 2c, except for small portions of the Canadian provinces of Ontario and Quebec. In this study, the stage IV data are interpolated to the 3-km grid used in the WRF simulations. The stage IV product was used to evaluate the rainfall rates from 1 to 10 mm h<sup>-1</sup> using the equitable threat score (ETS; Schaefer 1990), which is computed using all points on the domain where stage IV data are available. For plan view verification of

the numerical simulations, composite reflectivity is used.

**3. Results: 29 June 2012**

On 29 June 2012, a particularly severe, long-lived bow echo–derecho event produced damaging straight-line winds across several midwestern and mid-Atlantic states. This mesoscale convective system (MCS) is an ideal candidate for examining the impact of lightning data assimilation for a number of reasons. First, the event was poorly forecast by operational models, with both the GFS and NAM (horizontal grid spacings of  $\Delta x = 27$  km and  $\Delta x = 12$  km, respectively) failing to forecast the MCS with any lead time, providing an opportunity for improving the forecast. Second, the MCS developed within an amorphous area of isolated thunderstorms on the morning of 29 June 2012, suggesting that model forecast quality can be improved by forcing

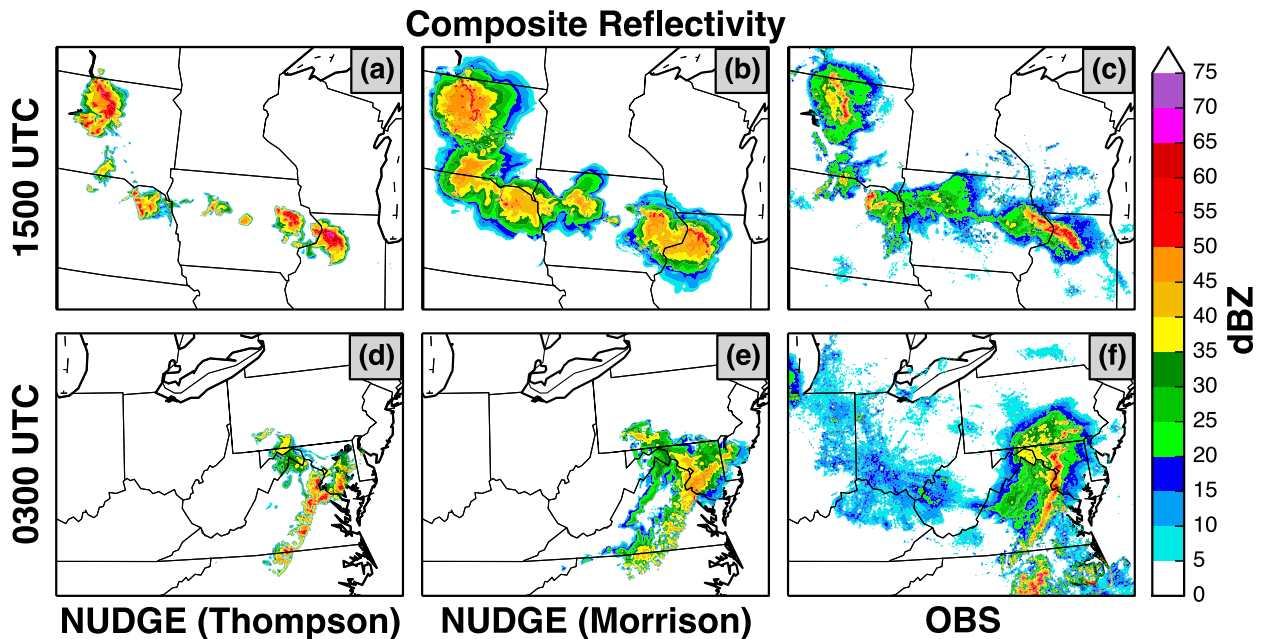


FIG. 9. Simulated and (right) observed composite reflectivity for the (bottom) forecast hour 3 (1500 UTC 29 Jun 2012) and (top) forecast hour 15 (0300 UTC 30 Jun 2012) of the deterministic simulations of the 29 Jun 2012 event for NUDGE with (left) Thompson and (middle) Morrison microphysics. The northwest (east central) portion of the model domain is displayed for forecast hour 3 (15).

the correct timing and placement of this convection. Third, the lack of obvious synoptic-scale lifting mechanisms to trigger the isolated thunderstorms in an unstable environment suggests that lowering the LCL and raising the CAPE where lightning is observed could encourage the formation of thunderstorms in the correct locations. It is worth noting that the experimental HRRR model, initialized at 1100 UTC 29 June 2012 and run at 3-km grid spacing, successfully forecasted the development of the derecho, and that the HRRR assimilates radar reflectivity and short-range lightning-flash-rate observations (Weygandt et al. 2008).

#### a. Lightning

Between 1200 and 1500 UTC 29 June 2012, WWLLN observed 4317 lightning strikes within the WRF domain described above. Location data from 4315 lightning strikes were assimilated using the observation nudging technique described in section 2 (two lightning strikes were filtered out; Fig. 2). The lightning strikes over eastern Iowa and western Illinois are associated with the thunderstorms that organized into the MCS.

#### b. Deterministic experiment

The average temporal change (from the beginning to the end of the 5-min period) in integrated water vapor (IWV) at nudged grid points for each 5-min bin during the first three hours of the CNTRL and NUDGE

simulations is shown in Fig. 3a. In CNTRL, no nudging is performed and average changes in IWV are nearly zero through the first three hours of the simulation. In NUDGE, noticeable increases in IWV occur through the first three hours, particularly over the first five minutes, when the average increase in IWV exceeds  $15 \text{ kg m}^{-2}$ . Subsequently, average increases in IWV hover around  $5 \text{ kg m}^{-2}$ . A similar result is found for the average change in CAPE at grid points where nudging is performed (Fig. 3b). In CNTRL, average changes in CAPE over each 5-min interval are nearly zero through the 3-h period. In NUDGE, substantial increases in CAPE occur at nudged locations, particularly over the first 15 minutes of the simulation, when increases in CAPE exceed  $2000 \text{ J kg}^{-1}$ . After that time, increases in CAPE over the 5-min intervals are modest compared to the initial period. Average condensate increases substantially during the first 60 minutes of the nudged simulation in comparison to the far lesser and slower increase in the control (Fig. 3c).

The impact of the nudging is evident in the simulated composite reflectivity fields (Figs. 4–7). Between 1200 and 1500 UTC 29 June 2012 (the first three hours of the simulations), the observed composite reflectivity indicates the development of thunderstorms along an east–west line across Iowa and eastern Nebraska that organize into a squall line in northwestern Illinois, while another line of thunderstorms, unrelated to the derecho event,

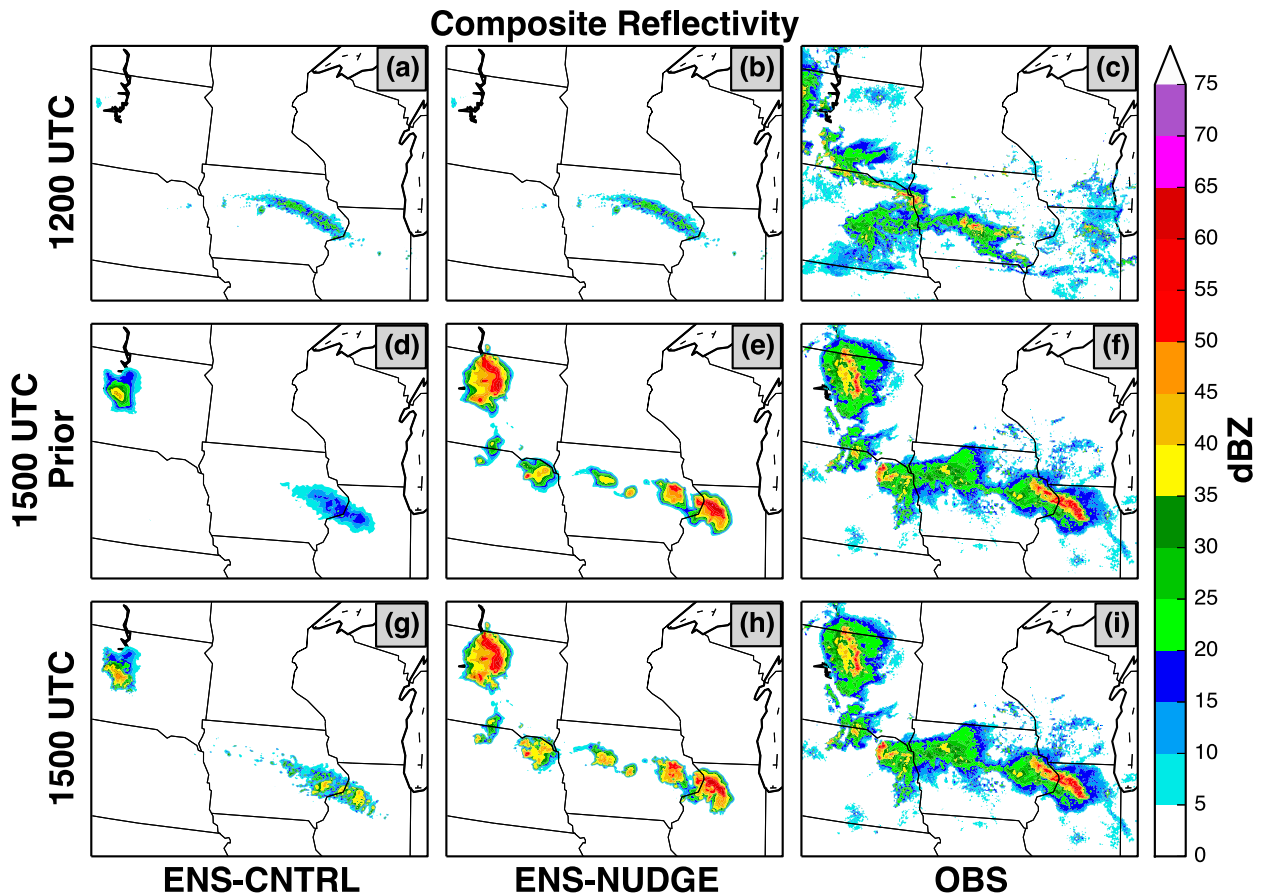


FIG. 10. Ensemble-mean and observed composite reflectivity (top row) after the 1200 UTC 29 Jun 2012 EnKF assimilation step and (middle row),(bottom row) before and after the 1500 UTC 29 Jun 2012 EnKF assimilation step, respectively. The columns correspond to (left) ENS-CNTRL, (center) ENS-NUDGE, and (right) observed reflectivity. The northwest portion of the model domain is displayed.

moves across central South Dakota (Figs. 4c,f,i). During these three hours, the CNTRL simulation does not produce thunderstorms over Iowa or Illinois, with limited thunderstorm development over central South Dakota and Nebraska (Figs. 4a,d,g). In the NUDGE simulation, nudging over this period forced or enhanced thunderstorm development in several locations, more closely reflecting observations (Figs. 4b,e,h). Throughout this period, the areas of highest reflectivity in NUDGE are larger in extent than observed. At 1500 UTC, there is a gap in the thunderstorms in NUDGE just west of the Illinois–Iowa border that is not present in the observations, a gap due to a lack of WWLLN lightning strikes in this portion of the line (Fig. 5). Overall, the convection in NUDGE is more consistent with observed reflectivity than in CNTRL, which is important because this convection develops into the derecho. In all simulated reflectivity fields, there is a notable lack of stratiform precipitation (e.g., behind the squall lines in South Dakota and Iowa in NUDGE) that may be due to the microphysics scheme being of two moment in only ice and rain (more below).

By 1800 UTC 29 June 2012, three hours after the nudging has ended, no convection associated with the MCS has initiated in the CNTRL simulation. In contrast, in the NUDGE simulation, thunderstorms propagated into east-central Illinois, although displaced to the southwest of the observed line (Figs. 6a–c). At 2100 UTC (Figs. 6d–f) in CNTRL, an MCS has formed across northern Illinois, far to the west of and oriented perpendicular to the observed MCS. In contrast, the MCS in NUDGE more closely resembles the observed MCS, exhibiting a similar orientation, with a slight westward displacement of the northern portion of the line. By 0000 UTC (Figs. 6g–i), CNTRL has produced an area of disorganized thunderstorms propagating in roughly the same direction as the observed MCS, but it is poorly oriented and west of the observed positions. In NUDGE a more realistic-looking MCS continues to propagate to the east-southeast, and is similar to the observed MCS in position and orientation.

Between 0300 and 0900 UTC 30 June 2012, the weakly organized line of storms in CNTRL is positioned west of

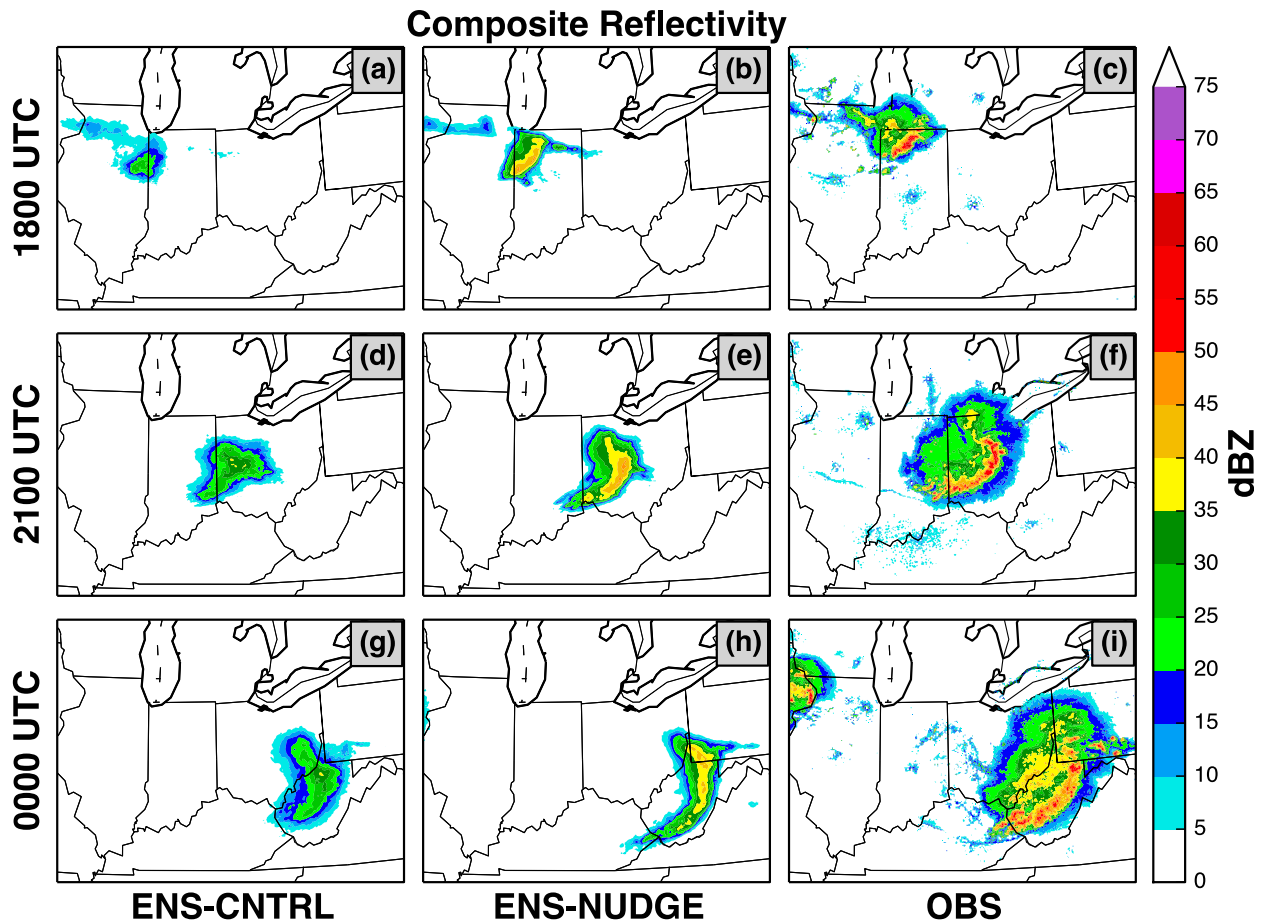


FIG. 11. As in Fig. 10, except results are displayed at 3-h intervals between 1800 UTC 29 Jun 2012 and 0000 UTC 30 Jun 2012. The central portion of the model domain is displayed.

the observed MCS and decays as it moves over the Appalachian Mountains (Fig. 7). At 0300 UTC in NUDGE, the northern end of the MCS has failed to maintain an organized structure, with the remainder of the line roughly matching the location of the observed convection (Figs. 7b,c). By 0600 UTC, the MCS in NUDGE has dissipated, while the observed MCS has moved to the eastern portion of the domain (Figs. 7e,f).

To evaluate the sensitivity of the abovementioned results to model configuration, we tested the use of a more computationally expensive fully double-moment microphysical scheme (Morrison) instead of Thompson microphysics scheme. Microphysics sensitivity studies of midlatitude squall lines suggest that full two-moment schemes facilitate the development of trailing stratiform precipitation behind convective lines (e.g., Morrison et al. 2009; Bryan and Morrison 2012; Baba and Takahashi 2014).

Figure 8 shows the ETS for precipitation equal to or exceeding  $1 \text{ mm h}^{-1}$ . Nudging improves upon the control

simulations for both the Thompson and Morrison microphysical schemes at virtually all times, with the greatest improvement after roughly 7 h. The Morrison scheme is modestly inferior between hours 0 and 8 due to regions of precipitation that are larger than observed (Figs. 9a–c). Between hours 12 and 18, the Morrison scheme produces trailing stratiform that more closely resembles the observations (Figs. 9d–f), but it exhibits only modestly superior ETS due to regions of precipitation in other portions of the domain that are larger than observed. Tests at other precipitation intensities are consistent with these results. Reducing the radius of lightning influence to 5 or 3 km did not significantly change the position of the convection and resulted in a slight intensification of maximum intensities. Changing the top of the nudging influence to 500 or 50 hPa had nearly no impact on the results. In another experiment, the initial nudging period was reduced from 3 to 1 h. Again, changes were small, with modest degradation of the phasing, structure, and amplitude during the middle

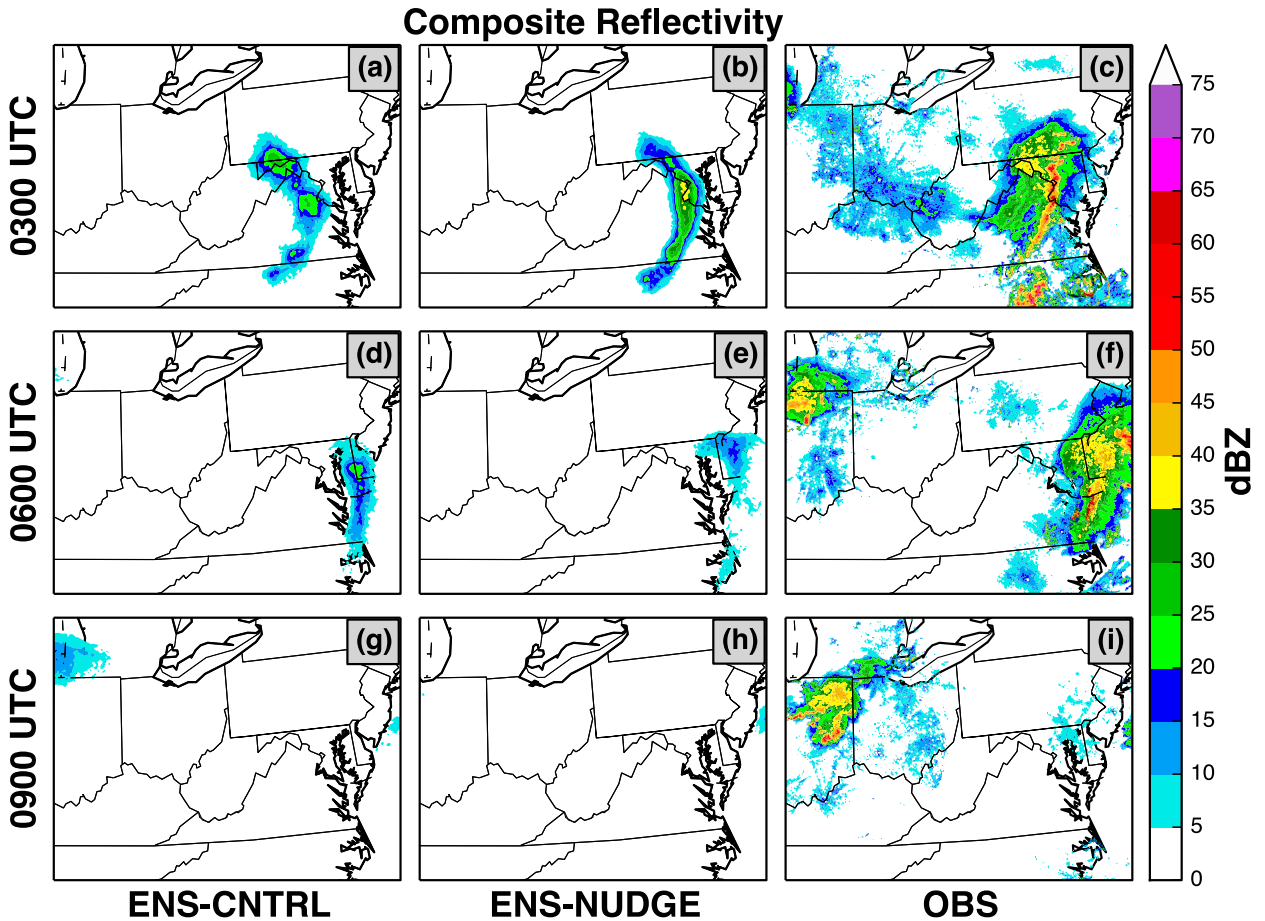


FIG. 12. As in Fig. 10, except results are displayed at 3-h intervals between 0300 UTC 30 Jun 2012 and 0900 UTC 30 Jun 2012. The central portion of the model domain is displayed.

part of the event for the 1-h nudging period. In each sensitivity experiment, the regions of high reflectivity values introduced in the assimilation period had a larger area than observed. In short, the results of these simulations were generally unaffected by large changes in simulation parameters, such as microphysical scheme, vertical extent of the nudging, radius of influence of the lightning, and period of nudging.

*c. Ensemble data assimilation experiment*

An important question regards the value of lightning assimilation when other mesoscale observations are present. To that end, WWLLN lightning data were assimilated along with a variety of additional observational assets for the June 2012 derecho. Specifically, an EnKF assimilation procedure is performed nine times (every three hours) between 1500 UTC 28 June and 1500 UTC 29 June 2012. At all times, less than 1.5% of the total observations are rejected, indicating that the ensembles did not suffer from filter divergence.

The impact of the nudging on the ensemble forecast is evident in the ensemble-mean composite reflectivity fields (Figs. 10–12). While these mean fields cannot provide the detail provided by a single ensemble member or a deterministic simulation because of the smoothing effects of the averaging, they indicate the degree of consensus among ensemble members regarding deep convection. Unlike the deterministic simulations, which are initialized with no water condensate, ensemble members develop thunderstorms during the 24-h spinup period prior to 1200 UTC 29 June 2012. At 1200 UTC 29 June 2012, before any lightning nudging has occurred, ENS-CNTRL and ENS-NUDGE are identical. In contrast to the deterministic simulations, convection is evident over Iowa at the end of the ensemble spinup period. Although there is agreement among ensemble members regarding the line of thunderstorms oriented in the east–west direction, the line is displaced north of the observed and is too narrow (Figs. 10a–c). At 1500 UTC 29 June 2012, prior to the

### ENS-NUDGE Composite Reflectivity 0000 UTC 30 June 2012

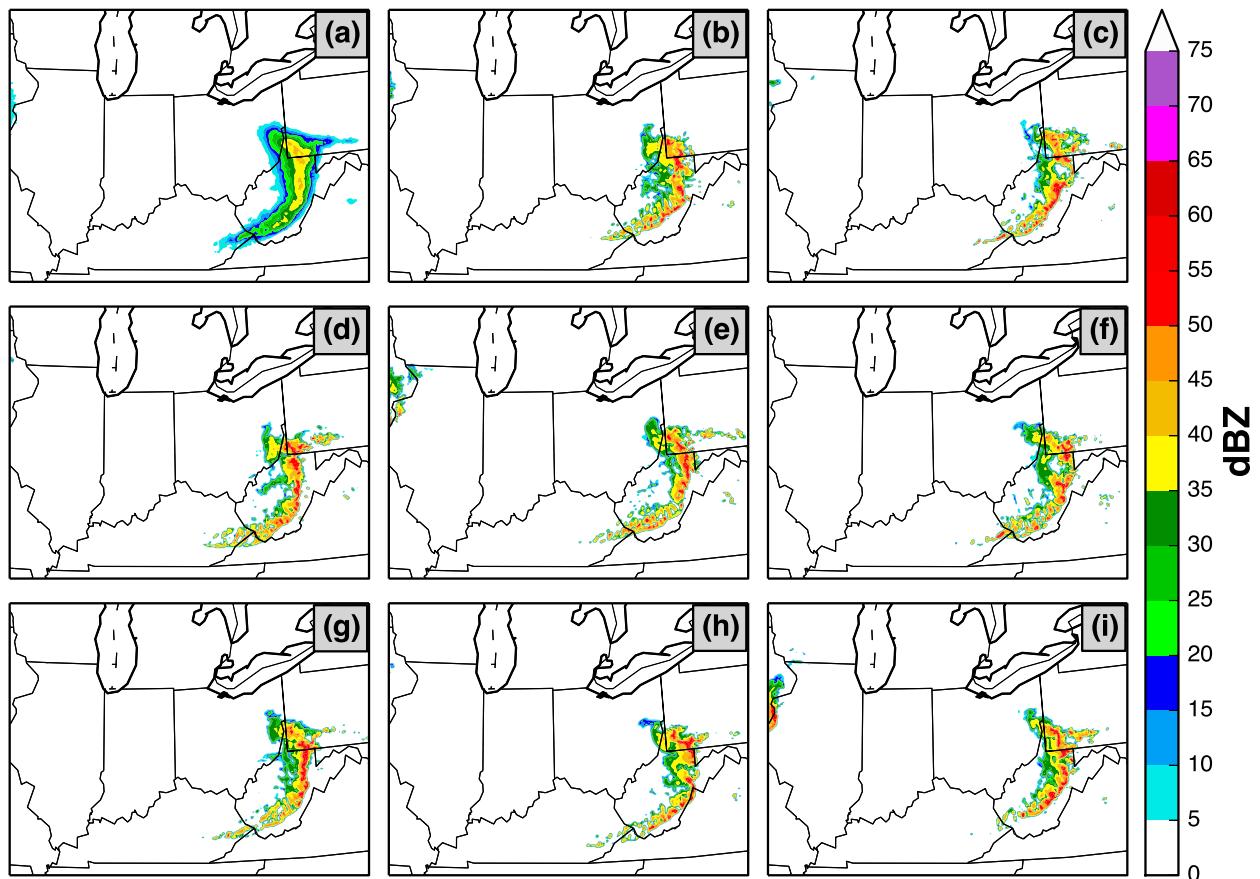


FIG. 13. Composite reflectivity from ENS-NUDGE at 0000 UTC 30 Jun 2012. (a) Ensemble-mean, and ensemble members (b) 1, (c) 6, (d) 11, (e) 16, (f) 21, (g) 26, (h) 31, and (i) 36. The central portion of the model domain is displayed.

EnKF assimilation but after the 3-h lightning nudging period, the line of thunderstorms in ENS-CNTRL remains stationary and fails to capture the storms in Nebraska and western Iowa. It also underplays the intensity of the storms in central South Dakota (Figs. 10d,f). In contrast, the lightning-based moisture nudging in ENS-NUDGE has forced the simulated thunderstorms to develop more consistently with observations (Figs. 10e,f). The effect of the EnKF assimilation step at 1500 UTC 29 June 2012 (using a variety of mesoscale observations) is to increase the ensemble-mean composite reflectivities of ENS-CNTRL, but it does not noticeably change the ensemble-mean composite reflectivities of ENS-NUDGE (Figs. 10g,h).

At 1800 UTC 29 June 2012, the ensemble-mean composite reflectivity of ENS-CNTRL indicates member agreement for thunderstorms in northwest Indiana, which are southwest of the observed line (Figs. 11a,c). At the same time, the ENS-NUDGE ensemble-mean

composite reflectivity possesses stronger convection that is positioned closer to the observations than ENS-CNTRL (Figs. 11b,c). At 2100 UTC 29 June 2012, ENS-CNTRL indicates convection in western Ohio that is more diffuse and less arc shaped than observed. In contrast, ENS-NUDGE produces a more realistic structure (Figs. 11d-f). At 0000 UTC 30 June 2012, the ensemble-mean composite reflectivity of ENS-CNTRL is weaker and westward compared to the observed reflectivity (Figs. 11g-i). Again, ENS-NUDGE produces a more realistic arc shape and higher reflectivities.

At 0300 UTC 30 June 2012, the MCSs in both ENS-CNTRL and ENS-NUDGE have decayed significantly, perhaps due to interactions with the Appalachian Mountains. There is greater consensus regarding the location of the MCSs among the members of ENS-NUDGE, which are also closer to the observed location of the MCSs than in ENS-CNTRL (Figs. 12a-c). By 0600 UTC 30 June 2012, most of the observed MCSs have moved outside of

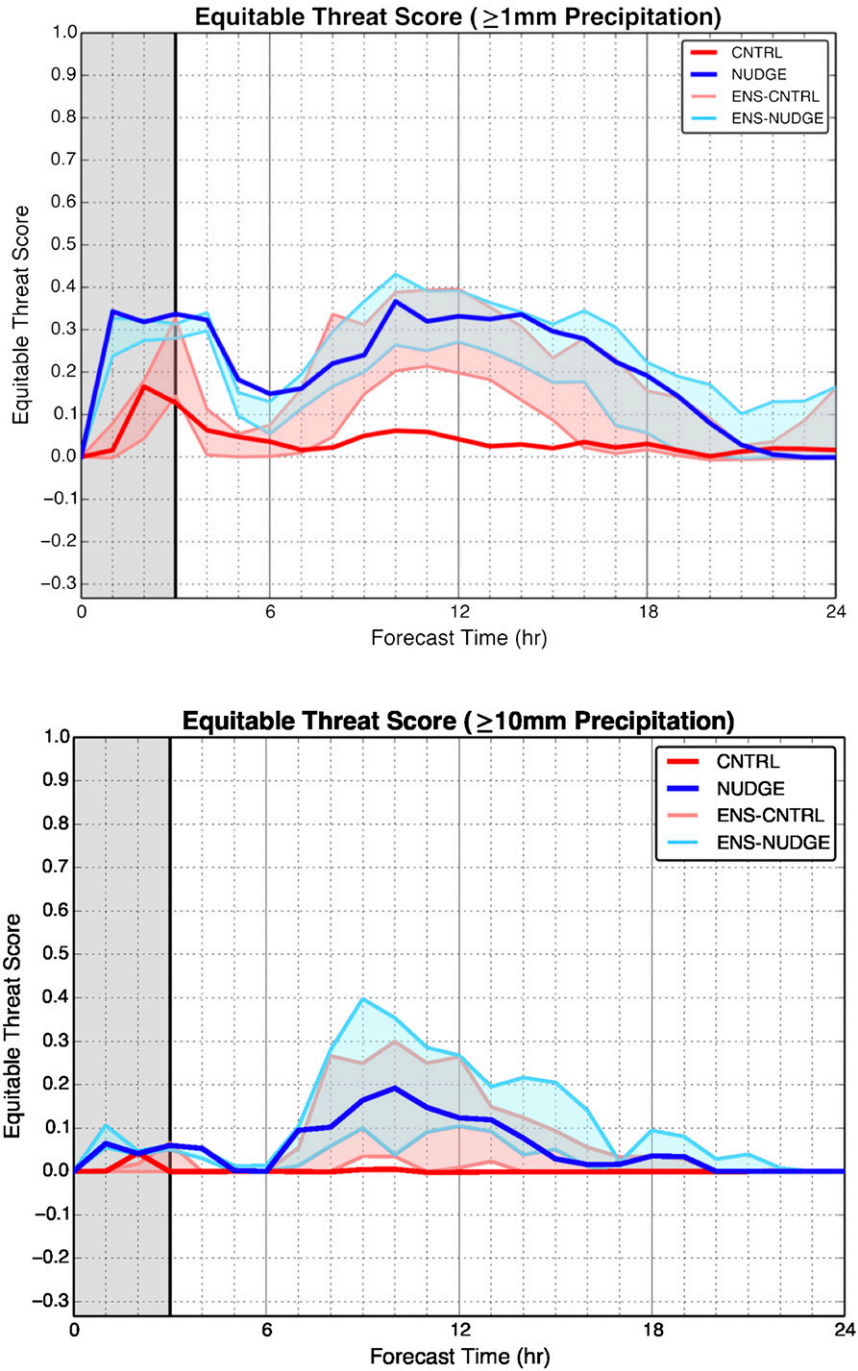


FIG. 14. Time series of ETS for CNTRL (thick red line), NUDGE (thick blue line), ENS-CNTRL (light red shaded region), and ENS-NUDGE (light blue shaded region) for the 29 Jun 2012 event for (top)  $\geq 1$  and (bottom)  $\geq 10$  mm over the previous hour. The vertical gray shaded area indicates times of moisture nudging in the NUDGE and ENS-NUDGE simulations.

the domain, with both ensemble predictions underplaying the intensity of the convection (Figs. 12d–f). At 0900 UTC 30 June 2012, the MCS is outside of the domain in ENS-CNTRL, ENS-NUDGE, and the observations

(Figs. 12g–i). Neither the control nor nudged ensemble forecasts predicted the observed strong convection over Indiana at the end of the simulation (e.g., 0600 UTC 30 June 2012).

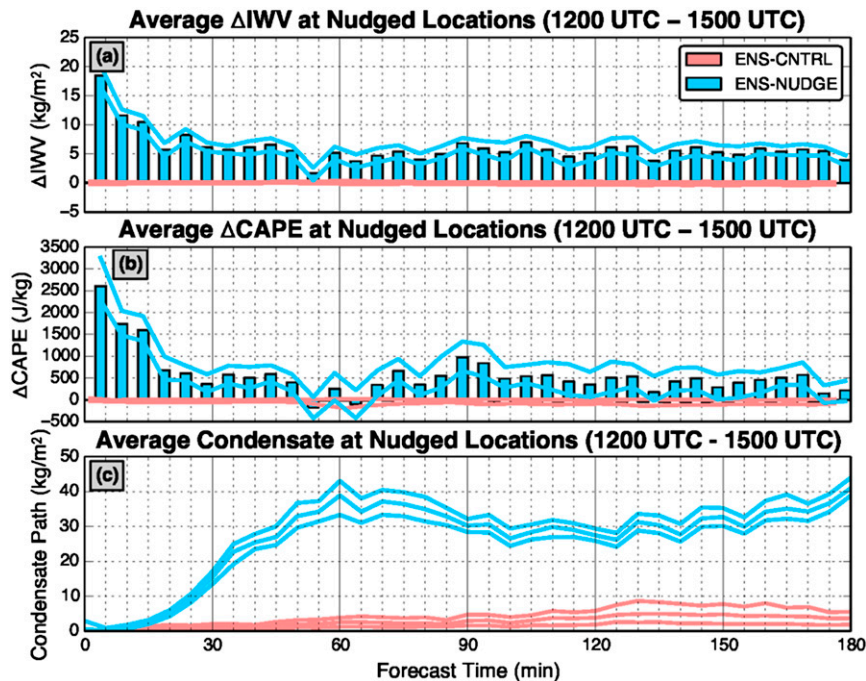


FIG. 15. Average temporal changes in (a) IWV and (b) CAPE at grid points where nudging is performed in ENS-NUDGE for the ensemble simulations of the 29 Jun 2012 event. (c) Average column condensate (liquid and solid water path) at nudged locations. Red bars (barely visible) and lines represent ensemble mean and range from ENS-CNTRL, while blue bars and lines represent ensemble mean and range from ENS-NUDGE.

An important question regards the variability among the ensemble members in the simulations nudged with WWLLN lightning (ENS-NUDGE). Figure 13 shows simulated reflectivities from the ensemble mean and eight ensemble members (1, 6, 11, 16, 21, 26, 31, 36) from ENS-NUDGE at 0000 UTC 30 June 2012. The individual members have more defined structures than the ensemble mean, with high reflectivities of the main convective line, but have similar structures and positions. Clearly, the assimilated observations are a strong constraint for these simulations.

Time series of ETS for the members of ENS-CNTRL and ENS-NUDGE, as well as the deterministic CNTRL and NUDGE simulations, are shown in Fig. 14 for both the 1 and 10  $\text{mm h}^{-1}$  precipitation thresholds. The low ETS values may be attributed to the conservative nature of the point-by-point comparison of this metric, as small location errors result in false alarms and misses. First, consider the lower (1 mm) precipitation threshold. With the sole exception of the last three hours, the deterministic nudged run has a substantially higher equitable threat score than the deterministic control simulation. In contrast, the differences in between the ensemble runs are much smaller. Between 1200 and 1500 UTC 29 June 2012 (hours 0 to 3 in the figure,

shaded), the moisture nudging forces thunderstorm development in all members of ENS-NUDGE, resulting in ETS exceeding those of ENS-CNTRL. The sudden increase in the maximum ENS-CNTRL ETS values at hour 3 (1500 UTC 29 June 2012) is due to the observed line of thunderstorms over the Illinois–Iowa border being collocated with the stationary line of thunderstorms in ENS-CNTRL that persisted between 1200 and 1500 UTC 29 June 2012 (Figs. 10a,d,g). At hour 6 (1800 UTC 29 June 2012), both ensembles forecast precipitation too far southwest of the observed precipitation in northwest Indiana (Figs. 10a–c). The corresponding decrease in ETS values is less dramatic in ENS-NUDGE, since the displacement error is less than in ENS-CNTRL. Between the hours 9 and 12 (2100 UTC 29 June and 0000 UTC 30 June 2012), the ETS values for both ensembles increase, as the MCS in both falls within the large region of observed rainfall (Figs. 11d–i). Between hours 12 and 18 (0000 and 0600 UTC 30 June 2012), the ETS values for both ensembles steadily decrease due to the decay of the simulated MCS as it crossed the Appalachian Mountains (Figs. 12a–f). Between hours 18 and 21 (0600 and 0900 UTC 30 June 2012), the decrease in ETS reflects the motion of the MCS out of the domain (Figs. 12g–i). The increase in the

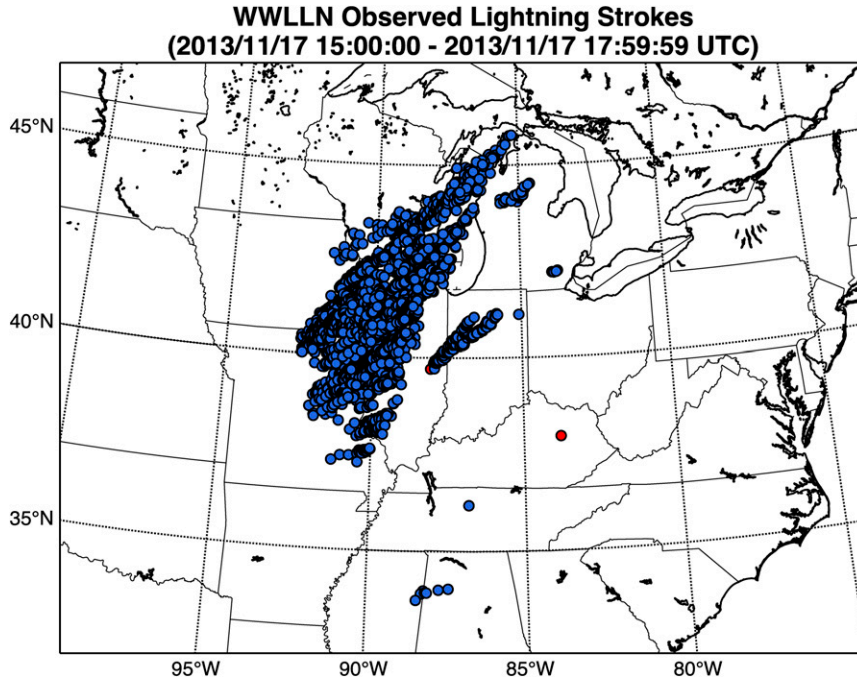


FIG. 16. Lightning strikes observed by WWLLN between 1500 and 1800 UTC 17 Nov 2012 on the WRF domain described in section 2c. Location data from 6071 lightning strikes were assimilated in the NUDGE simulation (blue dots). Four lightning strikes were removed from by the filtering technique described in section 2a (red dots).

upper end of the range of ETS values in ENS-CNTRL during the final three hours is due to some members of ENS-CNTRL accurately locating precipitation in eastern Iowa (not shown).

The ETS is considerably reduced for the 10 mm h<sup>-1</sup> threshold. There is very little skill for the nonnudged control, with substantial improvement for most hours with lightning nudging. As with the 1-mm threshold, the use of ensembles produces modest improvements without nudging and small but noticeable gains using nudging. The value of moisture nudging is limited to the middle period of the simulation, roughly from hours 6 to 18. In summary, nudging with WWLLN lightning substantially improves the deterministic model ETS at nearly all times. In contrast, in the ensemble (EnKF) data assimilation experiment, the improvement is more modest and limited to the period in which the derecho was over Indiana, Ohio, and West Virginia.

Further insights into the impact of lightning on the ensembles is provided in Fig. 15, which shows the average changes in IWV, CAPE, and condensate for ENS-CNTRL and ENS-NUDGE simulations during the 3-h nudging period. ENS-NUDGE shows a large increase during the initial 15 min, followed by modest increases for the remainder of the period. The range of the ensemble members (blue lines) is relatively small, reflecting the similarities of

the moisture-nudged solutions. Changes in average CAPE have a similar temporal progression, with the largest increases during the first 15 minutes, with a slightly larger range. Finally, there is a substantial change in average condensate for ENS-NUDGE during the first hour, with a relatively small variation among members. In contrast, the control shows very small growth during the 3-h period. In summary, nudged ensemble members evince very similar changes in IWV, CAPE, and condensate during the initial 3-h period, with a large ramp up during the first hour.

**4. Results: 17 November 2013**

To evaluate the generality of the lightning nudging approach described above, a substantially different event over the U.S. Midwest was examined. The November 2013 event provides the opportunity to examine the impacts of lightning data assimilation on the analysis and forecast of a synoptically well-resolved event. On 17 November 2013, a deepening cyclone and associated cold front moved across the Midwest, producing numerous supercells and squall lines across Illinois, Missouri, Iowa, and Wisconsin. A coherent line of convection formed along the cold front, extending from the Great Lakes into the northern portions Alabama and Mississippi. The event was accompanied by numerous reports of tornadoes

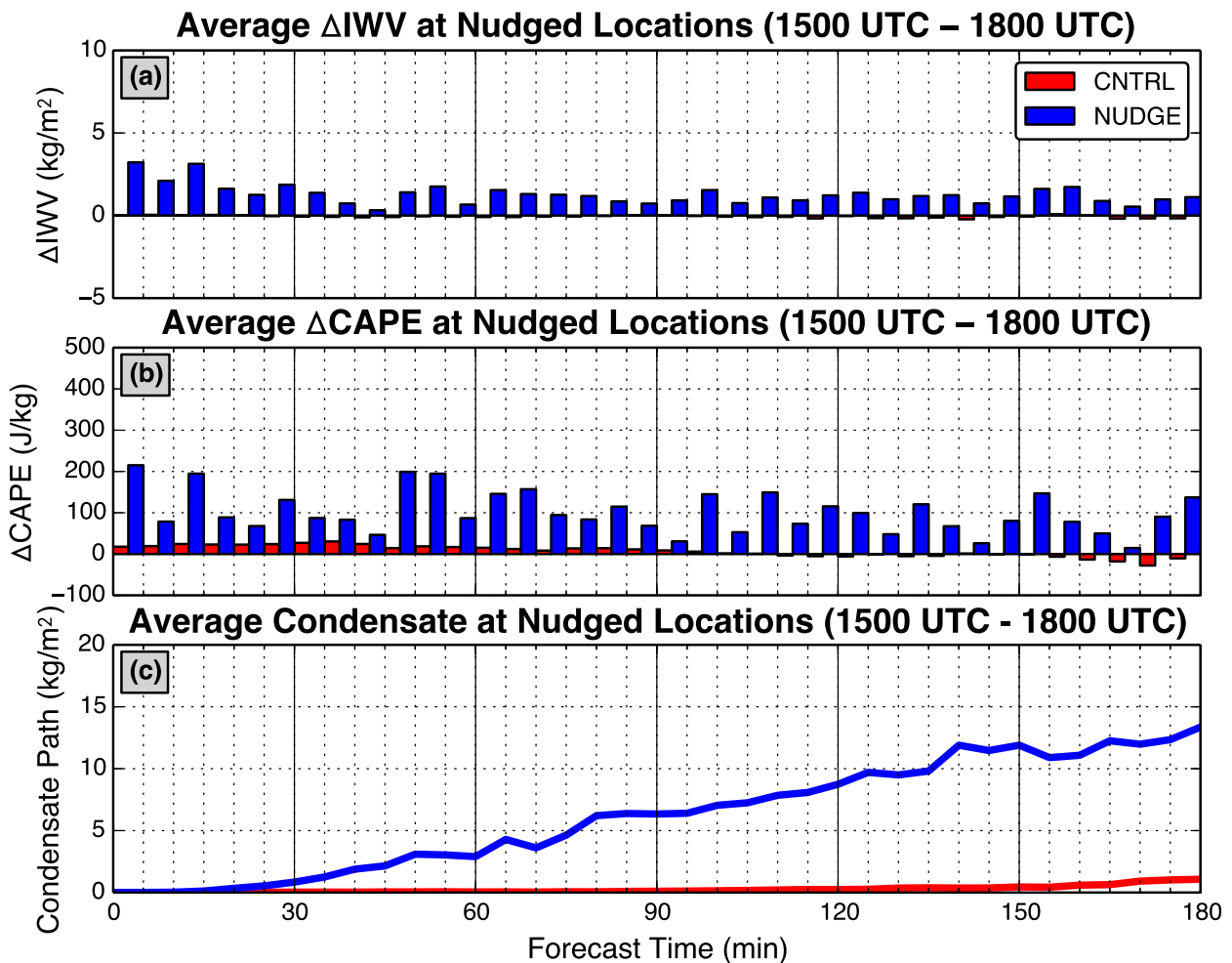


FIG. 17. Average temporal changes in (a) IWV and (b) CAPE at grid points where nudging is performed in NUDGE for the 17 Nov 2013 event. (c) Average column condensate (liquid and solid water path) at nudged locations. Red bars (barely visible) and lines represent results from CNTRL, while blue bars and lines represent results from NUDGE.

and straight-line wind damage across the Midwest. Unlike the 29 June 2012 event, this convective activity was forced by an obvious synoptic-scale feature, a cold front associated with an intensifying cyclone.

#### a. Lightning

Between 1500 and 1800 UTC 17 November 2013, WLLN observed 6075 lightning strikes within the WRF domain described in section 2c. Location data from 6071 lightning strikes were assimilated using the observation nudging technique described in section 2 (four lightning strikes were filtered out; Fig. 16). The assimilated lightning strikes are associated with the first cells that initiated along and ahead of the cold front.

#### b. Deterministic experiment

The average change in IWV at nudged grid points for each 5-min bin during the first three hours of the CNTRL

and NUDGE simulations is shown in Fig. 17a. In CNTRL, no nudging is performed and average changes in IWV are minimal during the first three hours of the simulation. In contrast, in NUDGE there are 1–3 kg m<sup>-2</sup> increases in IWV occurring during that period, with the largest values during the first 15 minutes. The average change in maximum CAPE at grid points where nudging is performed (Fig. 17b) indicates average changes in CAPE are nearly zero through the 3-h period in CNTRL, while in NUDGE increases in CAPE occur at nudged locations through the first three hours. Note that the average increases in IWV and CAPE at nudged points is much smaller for this case than in the 29 June 2012 event, likely due to colder atmospheric temperatures. For NUDGE, the average water condensate at nudged locations increases more gradually than in the 29 June 2012 case (Fig. 17c).

The impact of nudging is apparent in the simulated composite reflectivity fields. Between 1500 and 1800 UTC

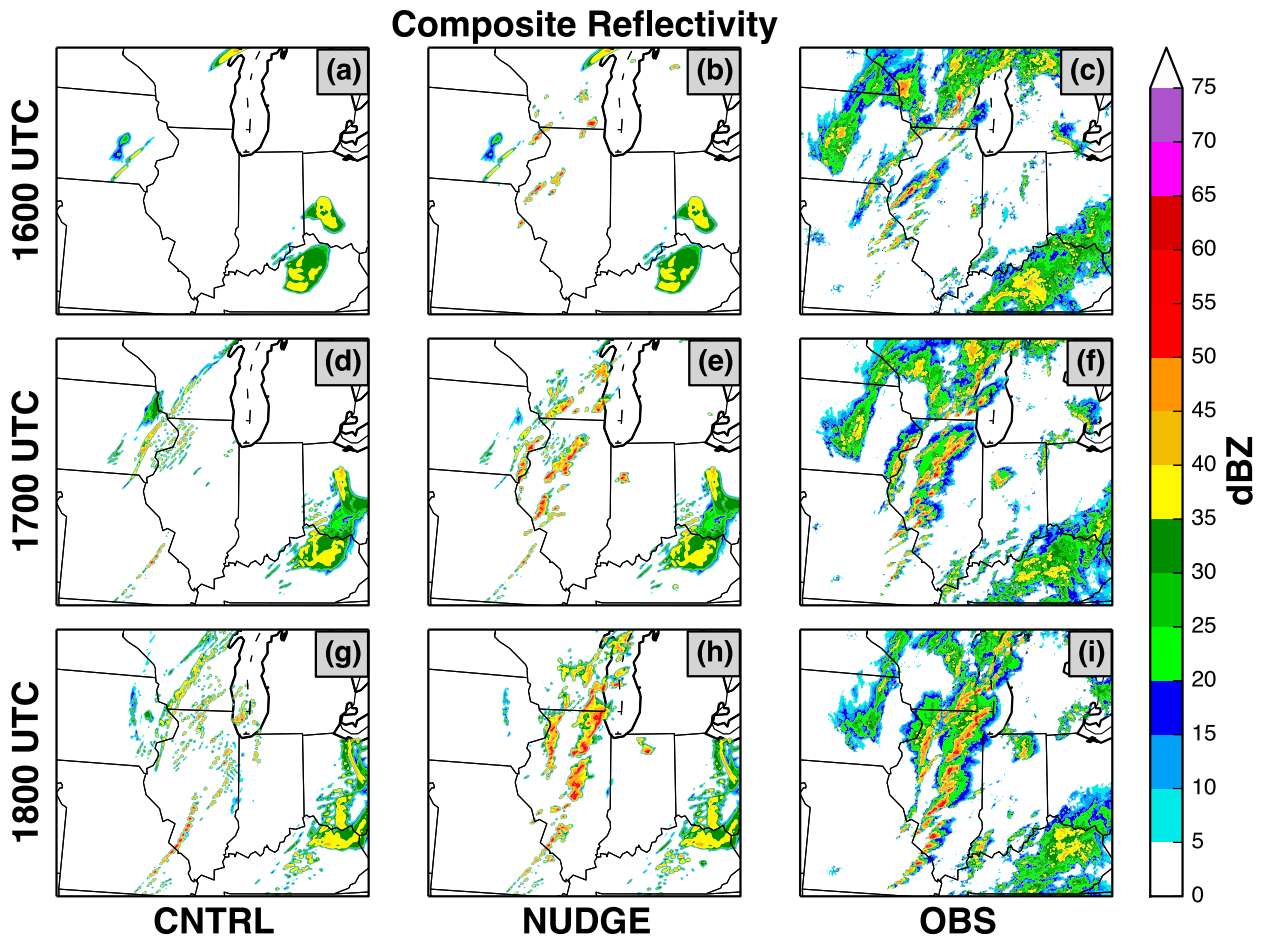


FIG. 18. Simulated and observed composite reflectivity for (top to bottom) the first three hours of the deterministic simulations of the 17 Nov 2013 event (1600–1800 UTC 17 Nov 2013) for (left to right) CNTRL, NUDGE, and observations. The north central portion of the model domain is displayed.

17 November 2013 (the first three hours of the simulations), the CNTRL simulation develops weak scattered thunderstorms across Illinois and Wisconsin, as well as larger, discrete cellular thunderstorms in Missouri and southern Illinois (Figs. 18a,d,g). CNTRL fails to capture the formation of observed lines of convection over northern Illinois (Figs. 18c,f,i). During the same period, NUDGE develops lines of more intense thunderstorms across northern Illinois and southern Wisconsin, as well as an isolated thunderstorm in Indiana that more closely match the observed structure and intensity, including the suggestion of the observed double line over Illinois (Figs. 18b,e,h).

At 2100 UTC 17 November 2013, three hours after the nudging has ended, the observed showers and thunderstorms that extended meridionally across Michigan were absent in CNTRL but appear in NUDGE (Figs. 19a–c). At 0000 UTC 18 November 2013, CNTRL forms a line of showers in northern Michigan, west of the line of

showers evident in NUDGE and the observations (Figs. 19d–f). At 0300 UTC 18 November, there is a westward lag in the northern extent of the line of showers in CNTRL compared to NUDGE, but there are no radar or precipitation observations in southern Canada for verification (Figs. 19g–i).

The time series of hourly ETS for this event show only subtle differences between CNTRL and NUDGE compared to the 29 June 2012 event for both the 1- and 10-mm thresholds (Fig. 20). In general, NUDGE was modestly superior for the majority of the simulation period, with improvements greater at 10 mm. Consistent with the more gradual development of storms in this event, the ETS of CNTRL and NUDGE diverge more slowly than for the 29 June 2012 event over the first three hours of the simulation. Subsequently, the difference in ETS is nearly constant until the frontal precipitation moves out of the domain (forecast hour 20; 1100 UTC 18 November 2013). The relatively small ETS differences

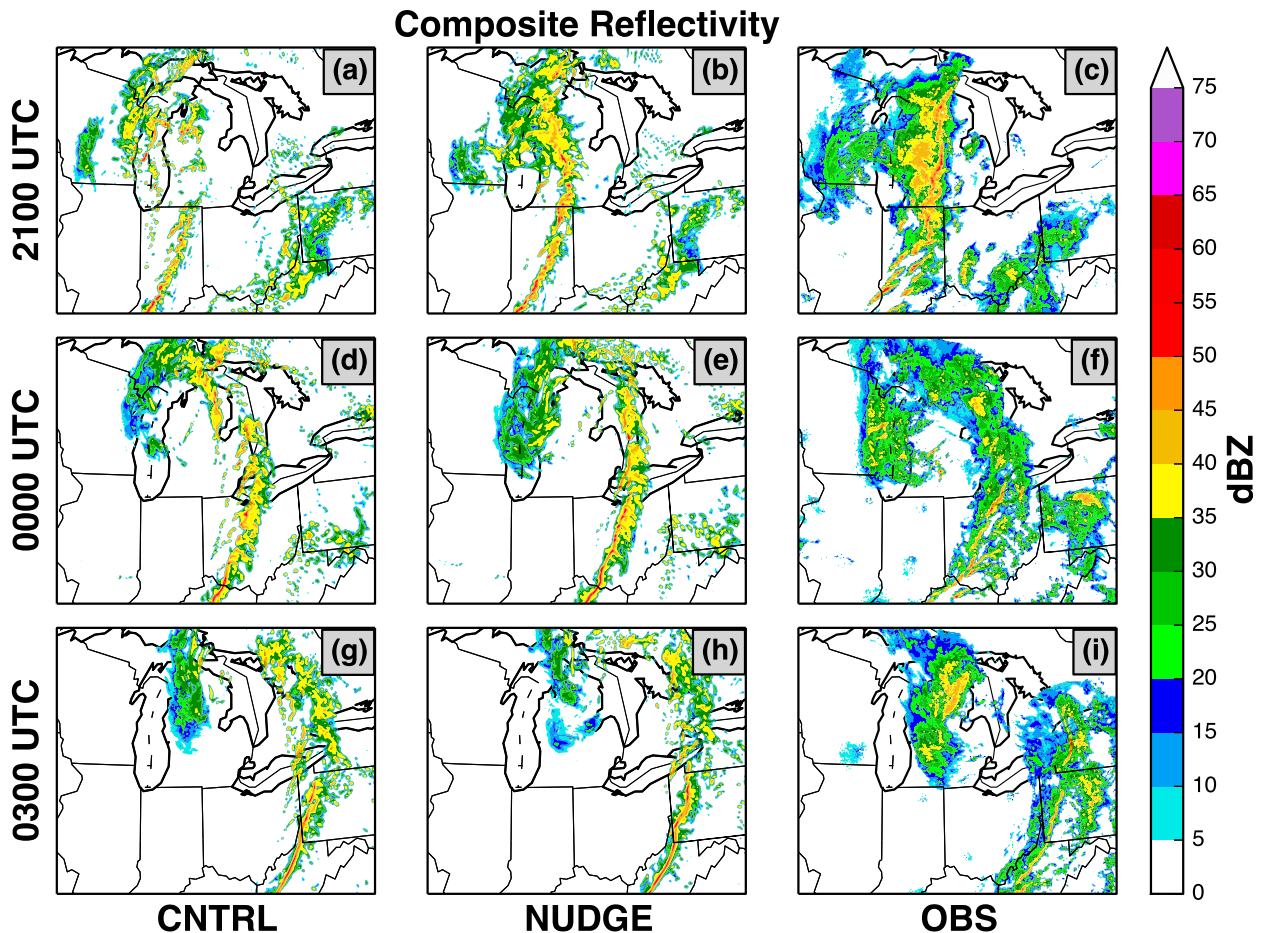


FIG. 19. As in Fig. 18, except results are displayed at 3-h intervals between 2100 UTC 17 Nov 2013 and 0300 UTC 18 Nov 2013. The north-central portion of the model domain is displayed.

between control and nudge simulations might be due to two factors: 1) the region impacted by nudging represents a small portion of the precipitation in the domain (compared to the June 2012 case) and 2) much of the nonconvective precipitation (which is represented by the 1-mm threshold) was well captured by the run without lightning assimilation.

## 5. Conclusions

In this work, a lightning assimilation approach is described and tested using data from the WWLLN and applied at convection-permitting (3 km) resolution. Specifically, this technique nudges the water vapor mixing ratio toward saturation within 10 km of a lightning observation throughout the troposphere and is more general than other approaches that require specific model microphysics or the use of flash rates. This approach was evaluated in both deterministic- and ensemble-based assimilation modes; specifically, the experiments were

run over the Midwest and the eastern United States for deterministic short-term numerical forecasts of the 29 June 2012 derecho and 17 November 2013 convective event and an ensemble prediction of the 29 June 2012 event. Although the goal of this research is to develop a general scheme applicable throughout the world, we have evaluated its impacts in a region in which meso-scale observations are relatively dense and detailed verification is possible.

Results from the deterministic simulations indicate that the lightning nudging technique increases integrated water vapor (IWV) and CAPE at locations where nudging is performed and improves the realism of the forecasts. For the 29 June 2012 event, the control simulation failed to simulate realistically the initiation and organization of convection and subsequently did not correctly forecast the organization, timing, and location of the observed derecho/mesoscale convective system (MCS). In contrast, the simulation with lightning assimilation triggered convection in the 3-h nudging

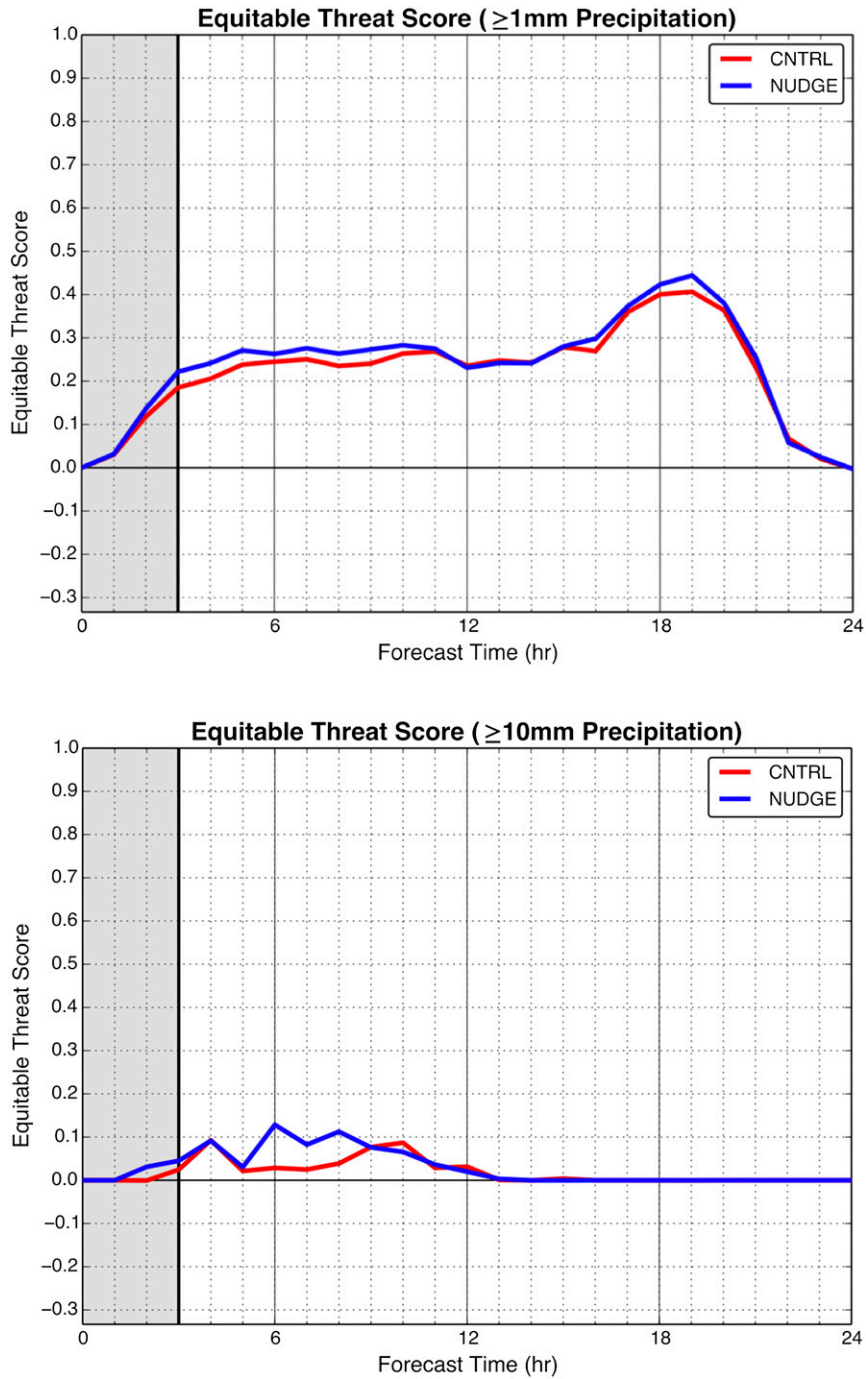


FIG. 20. Time series of ETS for CNTRL (thick red line) and NUDGE (thick blue line) for the 17 Nov 2013 event for both (top) 1- and (bottom) 10-mm thresholds. The vertical gray shaded area indicates times during which moisture nudging occurred in the NUDGE simulations.

period, leading to a substantially improved forecast. For the 17 November 2013 event, lightning nudging triggered thunderstorms ahead of a cold front in a realistic way; such thunderstorms were not produced in the control simulation. In neither case did the lightning

nudging degrade the forecast compared to the control simulation.

Since this study made use of a single microphysics scheme for all simulations, the Morrison double-moment scheme was tested; qualitatively, the results were similar,

with Morrison verifying slightly better. Other tests of the nudging period, vertical extent of nudging, and radius of influence suggested that the results presented above are robust. The regions of strong convection (large reflectivity) generated during the assimilation period appear larger in extent than observed in the 29 June 2012 case; this was not true for the 17 November 2013 case.

The application of the technique within an ensemble-based data assimilation and forecasting for the 29 June 2012 event improved the evolution of the convection during the lightning nudging period, although the impact on the subsequent forecast was less dramatic than in the deterministic simulations. The application of the nudging to the ensemble members reduced the spread of the predicted location of the convective line. The improvement in the forecasts between the deterministic and ensemble control simulations highlights the potential value of a high-resolution ensemble data assimilation and forecasting system (EnKF). The lesser impact of lightning nudging in the simulations with ensemble-based data assimilation suggests that the large volume of data assimilated into the high-resolution EnKF (aircraft, surface, maritime, radiosonde, and satellite-observed winds) can produce an accurate forecast of convective events even without lightning data. Since the eastern United States is heavily observed by those data sources, future work should evaluate lightning assimilation for locations where less data are available (e.g., over oceans, mountainous terrain, less populated regions) or reduce the density of observations. Radar reflectivity and precipitation observations from field campaigns and satellites such as the Tropical Rainfall Measuring Mission (TRMM) or the Global Precipitation Measurement (GPM) project could be used for verification in other regions. Further studies could also determine whether lightning data assimilation is most effective during specific seasons or periods.

Finally, the proposed method would probably be most effective in environments generally favorable to convection (e.g., substantial CAPE) but where instability or moisture is just below the necessary thresholds. Furthermore, this approach would probably be more useful when the model had no convection or convection over too small an area. If convection was already in place, then the area of interest would already be saturated, thus lessening the impact of this method.

*Acknowledgments.* The authors acknowledge use of the World Wide Lightning Location Network (<http://wwlln.net>), a collaboration among over 50 universities and institutions, for providing the lightning location data used in this paper. The authors also wish to thank the Data Assimilation Research Section of UCAR for its assistance

with DART and the Mesoscale and Microscale Meteorology Division of NCAR for its assistance with WRFDA. We also acknowledge high-performance computing support from the Yellowstone computer system provided by NCAR's Computational and Information Systems Laboratory, sponsored by the National Science Foundation. Three anonymous reviewers provided constructive suggestions that substantially improved this manuscript. This research was supported in part by NOAA Grant NA10OAR4320148.

## REFERENCES

- Abarca, S. F., K. L. Corbosiero, and T. J. Galarneau Jr., 2010: An evaluation of the Worldwide Lightning Location Network (WWLLN) using the National Lightning Detection Network (NLDN) as ground truth. *J. Geophys. Res.*, **115**, D18206, doi:10.1029/2009JD013411.
- Abreu, D., D. Chandan, R. H. Holzworth, and K. Strong, 2010: A performance assessment of the World Wide Lightning Location Network (WWLLN) via comparison with the Canadian Lightning Detection Network (CLDN). *Atmos. Meas. Tech.*, **3**, 1143–1153, doi:10.5194/amt-3-1143-2010.
- Alexander, G. D., J. A. Weinman, V. M. Karyampudi, W. S. Olson, and A. C. L. Lee, 1999: The effect of assimilating rain rates derived from satellites and lightning on forecasts of the 1993 Superstorm. *Mon. Wea. Rev.*, **127**, 1433–1457, doi:10.1175/1520-0493(1999)127<1433:TEOARR>2.0.CO;2.
- Anderson, J. L., 2001: An ensemble adjustment Kalman filter for data assimilation. *Mon. Wea. Rev.*, **129**, 2884–2903, doi:10.1175/1520-0493(2001)129<2884:AEAKFF>2.0.CO;2.
- , 2009: Spatially and temporally varying adaptive covariance inflation for ensemble filters. *Tellus*, **61A**, 72–83, doi:10.1111/j.1600-0870.2008.00361.x.
- Baba, Y., and K. Takahashi, 2014: Dependency of stratiform precipitation on a two-moment cloud microphysical scheme in mid-latitude squall line. *Atmos. Res.*, **138**, 394–413, doi:10.1016/j.atmosres.2013.12.009.
- Ballabrera-Poy, J., E. Kalnay, and S.-C. Yang, 2009: Data assimilation in a system with two scales—Combining two initialization techniques. *Tellus*, **61A**, 539–549, doi:10.1111/j.1600-0870.2009.00400.x.
- Bryan, G. H., and H. Morrison, 2012: Sensitivity of a simulated squall line to horizontal resolution and parameterization of microphysics. *Mon. Wea. Rev.*, **140**, 202–225, doi:10.1175/MWR-D-11-00046.1.
- Chang, D.-E., J. A. Weinman, C. A. Morales, and W. S. Olson, 2001: The effect of spaceborne microwave and ground-based continuous lightning measurements on forecasts of the 1998 Groundhog Day storm. *Mon. Wea. Rev.*, **129**, 1809–1833, doi:10.1175/1520-0493(2001)129<1809:TEOSMA>2.0.CO;2.
- Dowden, R. L., J. B. Brundell, and C. J. Rodger, 2002: VLF lightning location by time of group arrival (TOGA) at multiple sites. *J. Atmos. Sol.-Terr. Phys.*, **64**, 817–830, doi:10.1016/S1364-6826(02)00085-8.
- Evensen, G., 1994: Sequential data assimilation with a nonlinear quasi-geostrophic model using Monte Carlo methods to forecast error statistics. *J. Geophys. Res.*, **99**, 10 143–10 162, doi:10.1029/94JC00572.
- Fierro, A. O., and J. M. Reisner, 2011: High-resolution simulation of the electrification and lightning of Hurricane Rita during

- the period of rapid intensification. *J. Atmos. Sci.*, **68**, 477–494, doi:10.1175/2010JAS3659.1.
- , E. R. Mansell, C. L. Ziegler, and D. R. MacGorman, 2012: Application of a lightning data assimilation technique in the WRF-ARW model at cloud-resolving scales for the tornado outbreak of 24 May 2011. *Mon. Wea. Rev.*, **140**, 2609–2627, doi:10.1175/MWR-D-11-00299.1.
- , J. Gao, C. L. Ziegler, E. R. Mansell, D. R. MacGorman, and S. R. Dembek, 2014: Evaluation of a cloud-scale lightning data assimilation technique and a 3DVAR method for the analysis and short-term forecast of the 29 June 2012 derecho event. *Mon. Wea. Rev.*, **142**, 183–202, doi:10.1175/MWR-D-13-00142.1.
- Gaspari, G., and S. E. Cohn, 1999: Construction of correlation functions in two and three dimensions. *Quart. J. Roy. Meteor. Soc.*, **125**, 723–757, doi:10.1002/qj.49712555417.
- Goodman, S. J., and Coauthors, 2013: The GOES-R Geostationary Lightning Mapper (GLM). *Atmos. Res.*, **125–126**, 34–49, doi:10.1016/j.atmosres.2013.01.006.
- Hamill, T. M., J. S. Whitaker, and C. Snyder, 2001: Distance-dependent filtering of background error covariance estimates in an ensemble Kalman filter. *Mon. Wea. Rev.*, **129**, 2776–2790, doi:10.1175/1520-0493(2001)129<2776:DDFOBE>2.0.CO;2.
- Huang, X.-Y., and X. Yang, 2002: A new implementation of digital filtering initialization schemes for HIRLAM. Danish Meteorological Institute Tech. Rep. 53, 30 pp.
- Jacobson, A. R., R. Holzworth, J. Harlin, R. Dowden, and E. Lay, 2006: Performance assessment of the World Wide Lightning Location Network (WWLLN), using the Los Alamos Sferic Array (LASA) as ground truth. *J. Atmos. Oceanic Technol.*, **23**, 1082–1092, doi:10.1175/JTECH1902.1.
- Kain, J. S., and Coauthors, 2008: Some practical considerations regarding horizontal resolution in the first generation of operational convection-allowing NWP. *Wea. Forecasting*, **23**, 931–952, doi:10.1175/WAF2007106.1.
- Lin, Y., and K. E. Mitchell, 2005: The NCEP Stage II/IV hourly precipitation analyses: Development and applications. *19th Conf. on Hydrology*, San Diego, CA, Amer. Meteor. Soc., 1.2. [Available online at [https://ams.confex.com/ams/Annual2005/techprogram/paper\\_83847.htm](https://ams.confex.com/ams/Annual2005/techprogram/paper_83847.htm).]
- Liu, Y., A. Bourgeois, T. Warner, S. Swerdlin, and J. Hacker, 2005: Implementation of observation-nudging based FDDA into WRF for supporting ATEC test operations. *Extended Abstracts, Joint WRF/MM5 User's Workshop*, Boulder, CO, NCAR, 10.7. [Available online at <http://www2.mmm.ucar.edu/wrf/users/workshops/WS2005/abstracts/Session10/7-Liu.pdf>.]
- Lorenz, E., and K. A. Emanuel, 1998: Optimal sites for supplementary weather observations: Simulation with a small model. *J. Atmos. Sci.*, **55**, 399–414, doi:10.1175/1520-0469(1998)055<0399:OSFSWO>2.0.CO;2.
- Mansell, E. R., C. L. Ziegler, and D. R. MacGorman, 2007: A lightning data assimilation technique for mesoscale forecast models. *Mon. Wea. Rev.*, **135**, 1732–1748, doi:10.1175/MWR3387.1.
- Morrison, H., G. Thompson, and V. Tatarskii, 2009: Impact of cloud microphysics on the development of trailing stratiform precipitation in a simulated squall line: Comparison of one- and two-moment schemes. *Mon. Wea. Rev.*, **137**, 991–1007, doi:10.1175/2008MWR2556.1.
- Papadopoulos, A., T. Chronis, and E. N. Anagnostou, 2005: Improving convective precipitation forecasting through assimilation of regional lightning measurements in a mesoscale model. *Mon. Wea. Rev.*, **133**, 1961–1977, doi:10.1175/MWR2957.1.
- Pessi, A. T., and S. Businger, 2009: The impact of lightning data assimilation on a winter storm simulation over the North Pacific Ocean. *Mon. Wea. Rev.*, **137**, 3177–3195, doi:10.1175/2009MWR2765.1.
- Petersen, W. A., and S. A. Rutledge, 1998: On the relationship between cloud-to-ground lightning and convective rainfall. *J. Geophys. Res.*, **103**, 14 025–14 040, doi:10.1029/97JD02064.
- Saunders, C., 2008: Charge separation mechanisms in clouds. *Space Sci. Rev.*, **137**, 335–353, doi:10.1007/s11214-008-9345-0.
- Schaefer, J. T., 1990: The critical success index as an indicator of warning skill. *Wea. Forecasting*, **5**, 570–575, doi:10.1175/1520-0434(1990)005<0570:TCSIAA>2.0.CO;2.
- Skamarock, W. C., and Coauthors, 2008: A description of the Advanced Research WRF version 3. NCAR Tech. Note NCAR/TN-475+STR, 113 pp., doi:10.5065/D68S4MVH.
- Solomon, R., and M. Baker, 1998: Lightning flash rate and type in convective storms. *J. Geophys. Res.*, **103**, 14 041–14 057, doi:10.1029/97JD03323.
- Stauffer, D. R., and N. L. Seaman, 1994: Multiscale four-dimensional data assimilation. *J. Appl. Meteor.*, **33**, 416–434, doi:10.1175/1520-0450(1994)033<0416:MFDDA>2.0.CO;2.
- Thompson, G., P. R. Field, R. M. Rasmussen, and W. D. Hall, 2008: Explicit forecasts of winter precipitation using an improved bulk microphysics scheme. Part II: Implementation of a new snow parameterization. *Mon. Wea. Rev.*, **136**, 5095–5115, doi:10.1175/2008MWR2387.1.
- Torn, R. D., G. J. Hakim, and C. Snyder, 2006: Boundary conditions for limited-area ensemble Kalman filters. *Mon. Wea. Rev.*, **134**, 2490–2502, doi:10.1175/MWR3187.1.
- Weisman, M. L., W. C. Skamarock, and J. B. Klemp, 1997: The resolution dependence of explicitly modeled convective systems. *Mon. Wea. Rev.*, **125**, 527–548, doi:10.1175/1520-0493(1997)125<0527:TRDOEM>2.0.CO;2.
- Weygandt, S. S., S. G. Benjamin, M. Hu, T. G. Smirnova, and J. M. Brown, 2008: Use of lightning data to enhance radar assimilation within the RUC and Rapid Refresh models. *Third Conf. on Meteorological Applications of Lightning Data*, New Orleans, LA, Amer. Meteor. Soc., 8.4. [Available online at <https://ams.confex.com/ams/88Annual/webprogram/Paper134112.html>.]
- Williams, E. R., M. E. Weber, and R. E. Orville, 1989: The relationship between lightning type and convective state of thunderclouds. *J. Geophys. Res.*, **94**, 13 213–13 220, doi:10.1029/JD094iD11p13213.
- , T. Chan, and D. Boccippio, 2004: Islands as miniature continents: Another look at the land-ocean lightning contrast. *J. Geophys. Res.*, **109**, D16206, doi:10.1029/2003JD003833.